Clathrin promotes centrosome integrity in early mitosis through stabilization of centrosomal ch-TOG

Amy B. Foraker,[1,2,3,4] Stéphane M. Camus,[1,2,3,4] Timothy M. Evans,[1,2,3,4] Sophia R. Majeed,[1,2,3,4] Chih-Ying Chen,[1,2,3,4] Sabrina B. Taner,[1,2,3,4] Ivan R. Corrêa Jr.,[5] Stephen J. Doxsey,[6] and Frances M. Brodsky[1,2,3,4]

[1]Department of Bioengineering and Therapeutic Sciences, [2]Department of Pharmaceutical Chemistry, [3]Department of Microbiology and Immunology, and [4]The G.W. Hooper Foundation, University of California San Francisco, San Francisco, CA 94143
[5]New England Biolabs, Inc., Ipswich, MA 01938
[6]Program in Molecular Medicine, University of Massachusetts Medical School, Worcester, MA 01605

Clathrin depletion by ribonucleic acid interference (RNAi) impairs mitotic spindle stability and cytokinesis. Depletion of several clathrin-associated proteins affects centrosome integrity, suggesting a further cell cycle function for clathrin. In this paper, we report that RNAi depletion of CHC17 (clathrin heavy chain 17) clathrin, but not the CHC22 clathrin isoform, induced centrosome amplification and multipolar spindles. To stage clathrin function within the cell cycle, a cell line expressing SNAP-tagged clathrin light chains was generated. Acute clathrin inactivation by chemical dimerization of the SNAP-tag during S phase caused reduction of both clathrin and ch-TOG (colonic, hepatic tumor overexpressed gene) at metaphase centrosomes, which became fragmented. This was phenocopied by treatment with Aurora A kinase inhibitor, suggesting a centrosomal role for the Aurora A–dependent complex of clathrin, ch-TOG, and TACC3 (transforming acidic coiled-coil protein 3). Clathrin inactivation in S phase also reduced total cellular levels of ch-TOG by metaphase. Live-cell imaging showed dynamic clathrin recruitment during centrosome maturation. Therefore, we propose that clathrin promotes centrosome maturation by stabilizing the microtubule-binding protein ch-TOG, defining a novel role for the clathrin–ch-TOG–TACC3 complex.

Introduction

Clathrin-mediated pathways are required for normal mitotic progression and cytokinesis in vertebrate and slime mold cells (Niswonger and O'Halloran, 1997; Feng et al., 2002; Royle et al., 2005; Schweitzer et al., 2005; Boucrot and Kirchhausen, 2007; Lin et al., 2010; Royle, 2012). Multinucleated cells and abscission defects are generated by clathrin disruption through RNAi, genetic deletion, and expression of dominant-negative fragments, which have been analyzed in the context of accumulated rounds of mitosis. Clathrin's roles in the cell cycle have been ascribed to mitotic spindle stabilization (Royle et al., 2005; Royle and Lagnado, 2006; Fu et al., 2010; Lin et al., 2010; Booth et al., 2011) as well as to endosomal membrane traffic needed for cell expansion and abscission (Niswonger and O'Halloran, 1997; Feng et al., 2002; Thompson et al., 2002; Schweitzer et al., 2005; Boucrot and Kirchhausen, 2007). RNAi studies also implicate several clathrin-associated proteins in centrosome formation (Thompson et al., 2004; Lehtonen et al., 2008; Liu and Zheng, 2009; Shimizu et al., 2009). Disruption of centrosome integrity can induce multinucleation and abscission defects, raising the questions addressed here of whether clathrin itself is involved in centrosome function and, if so, which mitotic phenotypes result from disruption of which clathrin functions during the cell cycle. Here, we develop a new strategy for acute inactivation of clathrin within the time frame of the cell cycle to define distinct roles for CHC17 (clathrin heavy chain 17) and its isoform CHC22 in cell division and establish how interference with these pathways induces specific mitotic defects.

Clathrin is a cytosolic protein with a three-legged triskelion shape generated by trimerization of clathrin heavy chain (CHC) subunits. In interphase, triskelia assemble into lattices

Correspondence to Frances M. Brodsky: Frances.Brodsky@ucsf.edu

Abbreviations used in this paper: BG, benzylguanine; CHC, clathrin heavy chain; ch-TOG, colonic, hepatic tumor overexpressed gene; CLC, clathrin light chain; GAK, cyclin G–associated kinase; GAPDH, glyceraldehyde 3-phosphate dehydrogenase; GLA, glutaric acid; IF, immunofluorescence; IP, immunoprecipitation; SA, streptavidin; TfR, transferrin receptor.

The Rockefeller University Press $30.00
J. Cell Biol. Vol. 198 No. 4 591–605
www.jcb.org/cgi/doi/10.1083/jcb.201205116

that coat intracellular membranes by interaction with adaptor molecules (Brodsky et al., 2001). There are two CHC isoforms in vertebrates, CHC17 and CHC22, that share 85% sequence identity (Wakeham et al., 2005). CHC17 clathrin has a well-characterized role in endocytosis and sorting at the trans-Golgi network and endosomes. CHC17 also localizes to the mitotic spindle (Okamoto et al., 2000; Royle et al., 2005; Esk et al., 2010). CHC22 is most highly expressed in muscle, where it is involved in GLUT4 glucose transporter traffic (Vassilopoulos et al., 2009). In all cells, CHC22 functions in endosomal sorting at a distinct step from CHC17 and is not observed on the mitotic spindle under normal conditions (Esk et al., 2010). The CHC17 triskelion binds light chain subunits, which do not associate with the cellular form of CHC22 (Liu et al., 2001). Vertebrates have two exchangeable clathrin light chains (CLCs), LCa and LCb (Wakeham et al., 2005), that are expressed as nonneuronal or neuronal splice variants.

Studies to date make a compelling case for CHC17 clathrin playing a role in membrane traffic needed for cell division and a separate role in contributing to mitotic spindle stability. Although the status of clathrin-mediated endocytosis during early mitosis is debated (Sager et al., 1984; Schweitzer et al., 2005; Boucrot and Kirchhausen, 2007), it is agreed that from anaphase onset to cytokinesis exit, CHC17 clathrin functions in endosomal membrane-trafficking events that stabilize the equatorial cleavage furrow (Niswonger and O'Halloran, 1997; Gerald et al., 2001; Feng et al., 2002; Warner et al., 2006), provide membrane for pre-cytokinetic expansion (Boucrot and Kirchhausen, 2007), and contribute to midbody abscission (Thompson et al., 2002; Schweitzer et al., 2005; Prekeris and Gould, 2008; Joshi et al., 2010). Clathrin-coated vesicles at spindle poles have also been implicated in postmitotic Golgi reassembly (Radulescu and Shields, 2012). Recent studies of CHC17 indicate a direct role in stabilization of spindle microtubules through formation of a complex with TACC3 (transforming acidic coiled-coil protein 3) and ch-TOG (colonic, hepatic tumor overexpressed gene) (Fu et al., 2010; Hubner et al., 2010; Lin et al., 2010; Booth et al., 2011). These are nonmotor proteins that form a complex at minus and plus ends of microtubules and function in centrosome organization and stabilizing mitotic spindles (Gergely et al., 2000, 2003; Cassimeris and Morabito, 2004; Peset and Vernos, 2008). RNAi depletion of proteins known to bind CHC17, including the ARH (autosomal recessive hypercholesterolemia) adaptor (Lehtonen et al., 2008), epsin1 (Liu and Zheng, 2009), and cyclin G–associated kinase (GAK; Shimizu et al., 2009), disrupts centrosome maturation and integrity, suggesting CHC17 plays a role in centrosome function that could directly or indirectly influence later mitotic events.

In this study, we first use RNAi to deplete either CHC isoform to examine their comparative influence on centrosomes and cell division. We then selectively target CHC17 for acute inactivation in S phase or later in mitosis by transfecting cells with SNAP-tagged LCa that can be chemically cross-linked in situ (Lemercier et al., 2007). This strategy identified a novel function for CHC17 in centrosome maturation between S phase and the G2/M transition that, when disrupted, caused loss of centrosome integrity in metaphase and later mitotic defects. CHC22 function was not required for centrosome integrity, but its depletion caused multinucleation. Thus, multiple stages of cell division are influenced by specific clathrin functions.

Results

Depletion of CHC17 clathrin by RNAi affects centrosome number and morphology

A possible role for clathrin in centrosome maturation has been suggested by depletion of clathrin-interacting proteins (Lehtonen et al., 2008; Liu and Zheng, 2009; Shimizu et al., 2009). To investigate this, we analyzed centrosome morphology and number after RNAi-mediated depletion of CHC17, its associated CLCs (LCa and LCb), or the CHC22 isoform. These studies were performed in HeLa cells stably expressing GFP–α-tubulin (HeLa-GFP–α-tubulin) to visualize microtubule networks as well as immunolabeled centrosome proteins. After 72 h of treatment, siRNA against CHC17 reduced both CHC17 and CLCs by ≥50%, and codepletion of both CLCs caused partial reduction of CHC17 (Figs. 1 A and S1 B), consistent with known interdependence of clathrin subunits for their stability (Brodsky, 1985b; Ybe et al., 2007). The highest siRNA concentration (20 nM) targeting CLCs also led to an ∼50% reduction in CHC22, not unexpected because CHC22 expression indirectly depends on CHC17 pathways for its stability (Esk et al., 2010). CHC22 depletion resulted in ≥50% reduction of CHC22, with no significant effect on other clathrin proteins, as previously observed (Vassilopoulos et al., 2009; Esk et al., 2010). Effects of siRNAs were quantified in different HeLa clones compared with nonsilencing treatments (Fig. S1).

Centrosomes were visualized by immunofluorescence (IF) to detect centrosome proteins γ-tubulin (Fig. 1) and pericentrin-2 (PCNT2; Fig. 2) in prometaphase and metaphase cells after siRNA depletion (72 h) of clathrin components. Defects were obvious using both markers. Depletion of CHC17 or CLCs doubled the percentage of cells with either amplified centrosomes or multipolar spindles (more than two of each), whereas codepletion of CHC17 and CLCs quadrupled the defective population (Fig. 1, B and D). CHC17- and/or CLC-depleted cells also displayed signs of centrosome fragmentation (Fig. 2) as well as reduced or diffuse fluorescence intensity of centrosome proteins at spindle poles (Figs. 1 B and 2). Levels of γ-tubulin or PCNT2 in lysates of clathrin-depleted cells (Fig. S1 B and not depicted) were unaffected. Therefore, observed changes reflect altered subcellular localization of these centrosome components, not their altered protein stability. CHC22 depletion did not affect centrosome number or spindle nucleation (Fig. 1, C and D). Thus, CHC17 and associated CLCs, but not CHC22, mediate pathways that affect centrosome number, integrity, and subsequent spindle nucleation. Coincidence of multipolar spindles with centrosome integrity defects (Fig. 1 D) correlates with known pathways of spindle nucleation in mammalian cells (Lingle and Salisbury, 1999).

Centrosome numbers and morphology are determined by centriole duplication and centrosome maturation, which occur during G1/S- and G2/M-phase transitions, respectively (Sluder and Rieder, 1985; Azimzadeh and Bornens, 2007). HeLa cells

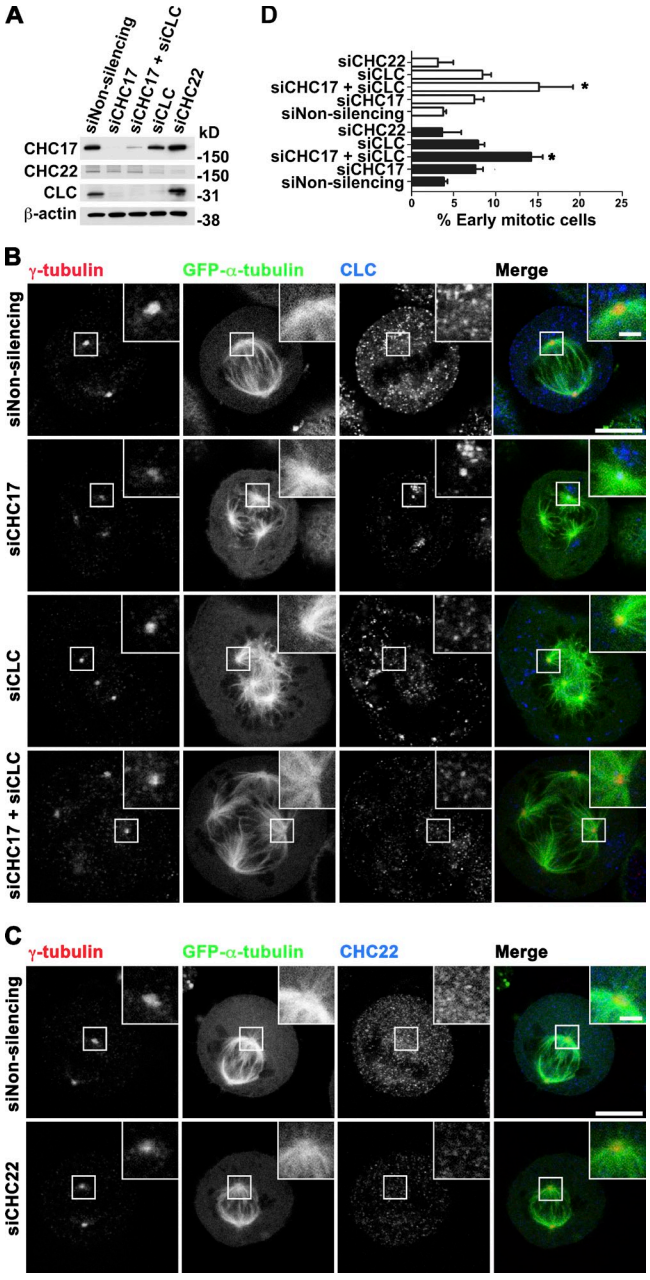

Figure 1. **Depletion of CHC17 clathrin amplifies mitotic centrosome number and induces multipolar spindle formation.** (A) HeLa-GFP–α-tubulin cells were treated (72 h) with siRNA-targeting CHC17, CLCs LCa and LCb (siCLC), CHC22, both CHC17 and CLC, or with nonsilencing siRNA (siNonsilencing). Cell lysates were analyzed for protein depletion by immunoblotting for proteins at the left. β-actin serves as a loading control. Molecular mass marker position is shown right. (B and C) HeLa-GFP–α-tubulin cells were treated with siRNA, as in A, and processed for IF to detect γ-tubulin and CLC or CHC22. GFP–α-tubulin was visualized in green. Red-green merge is yellow. Bars, 7.5 µm. (insets) Boxes in each frame are magnified threefold. Bars, 2.0 µm. All images are 2D. (D) The percentage of HeLa-GFP–α-tubulin cells with more than two centrosomes (shaded bars) and the percentage of cells with more than two spindle poles (open bars) were quantified for ≥200 mitotic cells in prometaphase or metaphase for each siRNA treatment. Centrosomes were identified by γ-tubulin staining at spindle poles. Occasional spindle poles without obvious centrosomes were observed, so these were scored separately. Data represent the mean ± SD of four to five independent experiments. Statistically significant results are shown in comparison with nonsilencing siRNA conditions (*, $P < 0.1$ based on a one-way analysis of variance Friedman's matched pairs test with Dunn's multiple comparison post-hoc test).

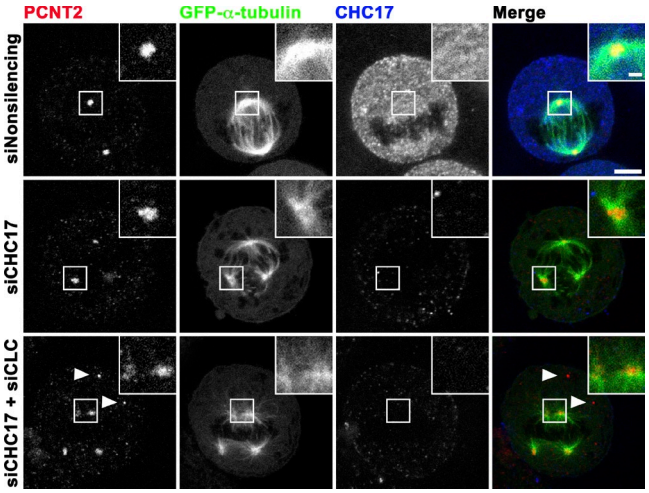

Figure 2. **Centrosome fragmentation is observed in early mitotic cells depleted for CHC17 and CLCs.** HeLa-GFP–α-tubulin cells treated (72 h) with siRNA, as indicated (left), were processed for IF to detect PCNT2 and clathrin (CHC17). GFP–α-tubulin was visualized in green. Red-green merge is yellow. Centrosome fragments, defined by PCNT2 staining, that are not localized to a spindle pole are indicated (arrowheads). Bar, 7.5 µm. (insets) Boxed regions are magnified threefold and highlight more diffuse PCNT2 staining at spindle poles in clathrin-depleted samples compared with the nonsilencing siRNA (siNonsilencing) treatment. Bar, 2 µm. All images are 2D.

stably expressing the centriolar protein centrin-2 (Salisbury et al., 2002) tagged with GFP (HeLa–centrin-2–GFP) were analyzed to determine whether effects of clathrin depletion on centrosomes could be explained by an effect on duplication. A slight, but not statistically significant, increase in cells with more than the expected four centrioles produced by normal duplication was observed upon depletion of CHC17 clathrin subunits (Fig. 3) compared with treatment with nonsilencing siRNA or siRNA-targeting CHC22. Levels of PCNT2 (not depicted), which can affect centriole amplification (Pihan et al., 2001) and levels of endogenous centrin-2 (Fig. 3 A), were not significantly altered upon any siRNA treatment. These observations suggest that CHC17 does not play a direct role in centriole duplication but may affect centrosome number through another pathway.

A block in cytokinesis can also cause centrosome defects (Lingle et al., 2005). Indeed, depletion of CHC17 resulted in a trend toward multinucleation after 48 or 72 h of siRNA treatment (Figs. 4 and S1 [A and B]), as previously reported (Royle et al., 2005). Depletion of CHC22, which did not cause centrosomal defects (Fig. 1), produced similar phenotypes of multinucleation, suggesting a distinct role for CHC22 in the cell cycle. Loss of either CHC did not produce the significant level of multinucleation seen after depletion of γ-tubulin, an established participant in cytokinesis (Fig. 4 B), and CLC depletion by itself had little effect on multinucleation. The latter observation is consistent with recent studies showing that, although CLC contributes to CHC17 stability and assembly control, CLC depletion does not mimic CHC17 depletion but mainly affects CLC regulation of actin associated with CHC17-coated membrane (Chen and Brodsky, 2005; Wilbur et al., 2008; Bonazzi et al., 2011).

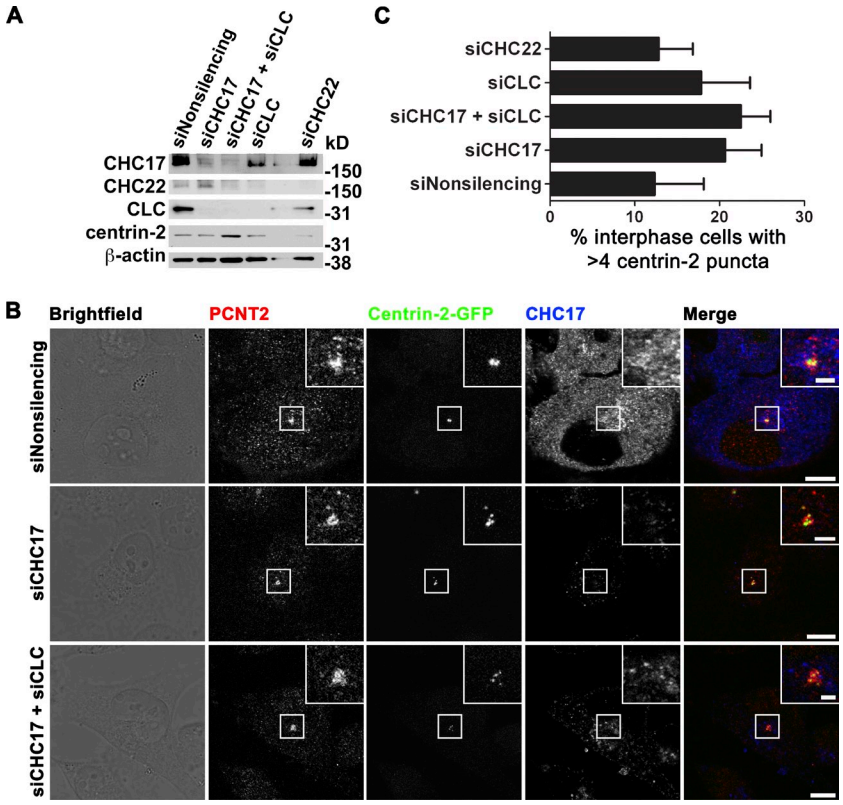

Figure 3. **Interphase centriole centrin-2 puncta are marginally increased by CHC17 and CLC depletion.** (A) HeLa–centrin-2–GFP cells were treated (72 h) with siRNA, as indicated (top). Depletion of proteins (left) was detected by immunoblotting siRNA-treated cell lysate. Molecular mass marker position is shown on the right. (B) HeLa–centrin-2–GFP cells were treated (72 h) with siRNA, as indicated (left), and then processed for IF to detect PCNT2 and CHC17. Centrin-2–GFP was visualized in green. Red-green merge is yellow. Bars, 10 µm. (insets) Boxes in each frame are magnified threefold. 2D confocal images are shown with the corresponding brightfield image. Bars, 2 µm. (C) The percentage of HeLa–centrin-2–GFP cells with more than four centrin-2 puncta per cell in interphase (representing G1, S, and G2 phases) was quantified for ≥50 cells for each siRNA treatment indicated. Centrin-2 puncta were identified by centrin-2–GFP that colocalized with PCNT2 detected by IF. Examples of interphase cells with more than two centrin-2 puncta are seen in B for the indicated siRNA treatments. Data represent the mean ± SEM for four independent experiments.

The most significant phenotype observed in these siRNA depletion studies was amplification of centrosome number by jointly targeting CHC17 and CLCs (Fig. 1). In addition, alteration of centrosome integrity and morphology and spindle multipolarity was observed (Fig. 2). Localization of CHC17 clathrin to centrosomes was not obvious in these samples (Figs. 1, 2, and 3) fixed by PFA. But, in samples fixed in methanol, CHC17 detected by antibodies to either the heavy or light chain subunits was observed to colocalize with the centrosomal markers PCNT2 and γ-tubulin in nontransfected HeLa cells (Fig. 5 A), suggesting the possibility that CHC17 functions directly at the centrosome.

Acute inactivation of CHC17 function using SNAP-tagged CLC

Although siRNA-based depletion indicates cell cycle–related clathrin functions, the relationship of these functions to phenotype is not possible to establish because two to three rounds of cell division occur during the period over which siRNA treatments are performed. Therefore, to investigate further how CHC17 clathrin might influence centrosomes and address whether cell cycle perturbations caused by clathrin depletion could arise from centrosomal defects, we developed an acute inactivation strategy based on the SNAP-tag technology (Gautier et al., 2008) to target CHC17 clathrin specifically. The SNAP-tag is a 20-kD protein derived from the human DNA repair enzyme O^6-alkylguanine–DNA alkyltransferase (Juillerat et al., 2003), which covalently binds O^6-benzylguanine (BG; Keppler et al., 2004) and its derivatives, many of which are cell permeable. Fluorescent BG derivatives label intracellular SNAP fusion proteins in live cells, whereas BG–glutaric acid (GLA)–BG covalently cross-links two proximal SNAP-tagged proteins when added to live cells (Lemercier et al., 2007). To use SNAP-tag–mediated cross-linking for acute clathrin inactivation, we transfected HeLa cells with a construct encoding ubiquitous (nonneuronal) LCa (uLCa) with the SNAP-tag at the N terminus (SNAP-uLCa, a 57-kD fusion protein) and selected a stable cell line, clone 3.3. The uLCa is the dominant isoform of CLCs in HeLa cells. CLCs compete with each other for CHC17 binding (Brodsky et al., 1987), so transfected CLCs readily replace endogenous CLCs (Acton et al., 1993), when expressed at higher levels, and excess CLCs are rapidly degraded (Brodsky, 1985b). Furthermore, CLCs do not bind to intracellular CHC22 (Liu et al., 2001), thus cross-linking SNAP-uLCa targets CHC17 but not CHC22 for inactivation.

To establish its normal behavior and potential to cross-link associated CHC17, the SNAP-tagged uLCa in clone 3.3 was shown to bind CHC17 by coimmunoprecipitation (co-IP; Fig. S2 A). Additionally, SNAP-uLCa, labeled with the BG-derivative SNAP-TMR-Star, colocalized with endogenous CHC17 in interphase cells and on the mitotic spindle (Fig. S2 B) in PFA-fixed cells. In methanol-fixed cells, the SNAP-uLCa colocalized clearly with centrosomal markers in interphase and metaphase (Fig. 5 B). The latter colocalization was specific, as endosomal markers transferrin receptor (TfR) or EEA1 (early endosomal antigen 1) did not localize to centrosomes (Fig. 5 C). When incubated with BG-GLA-BG, dimerization of the SNAP-tagged uLCa was readily detected (Fig. 6 A), and variation of time and concentration revealed that a 5–10-µM treatment for 2 h was sufficient for optimal cross-linking. After treatment with 5 µM BG-GLA-BG for 2 h, clone 3.3 cells were tested for uptake of fluorescent transferrin over 10 min and 1 h (Fig. 6, B and C).

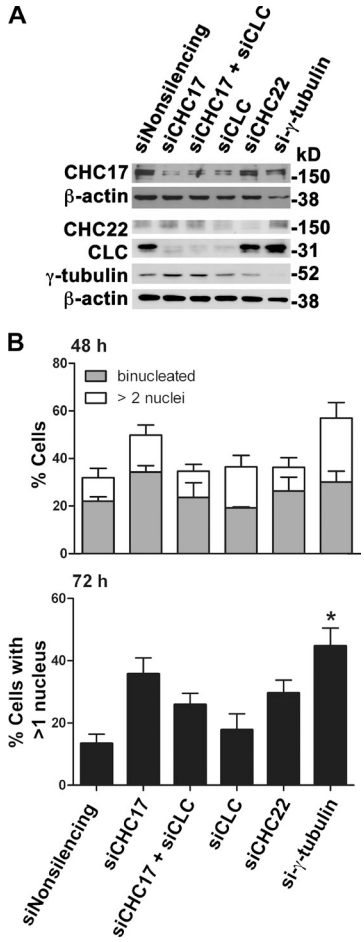

Figure 4. **Depletion of either CHC17 or CHC22 increases multinucleation.** (A) HeLa-GFP–α-tubulin cells were treated (48 h) with siRNA, as indicated (top). Lysates of treated cells were immunoblotted for the proteins indicated (left). Molecular mass marker position is shown on the right. (B) The percentage of binuclear and multinuclear cells was assessed at 48 or 72 h after each siRNA treatment indicated by nuclear staining with DAPI (>100 cells per treatment per experiment were scored). Targeted siRNA effects were compared with nonsilencing siRNA (siNonsilencing) effects for statistical significance. The mean ± SD of four to five independent experiments is shown (*, $P < 0.1$).

Compared with mock-treated cells, in which transferrin was observed in intracellular vesicles within 10 min, transferrin remained largely at the plasma membrane in BG-GLA-BG–treated cells, indicating disruption of clathrin-mediated endocytosis. After 1 h of transferrin uptake, mock-treated cells were almost completely clear of subcellular fluorescent transferrin, a sign of efficient recycling and some degradation. In contrast, cells treated with BG-GLA-BG showed fluorescent transferrin still present in vesicles labeled by IF for CHC17 and EEA1 (Fig. 6, B and C), reflecting diminished uptake of fluorescent transferrin and a block in its endosomal sorting or recycling. It is well documented that after blocking clathrin-mediated uptake, transferrin can be internalized by nonclathrin-mediated pathways and is then detected with clathrin in sorting endosomes (Damke et al., 1994; Bennett et al., 2001). Impaired uptake of TfR after exposure of clone 3.3 to cross-linker was further demonstrated using a cell surface biotinylation assay. Clone 3.3 cells that were treated with or without BG-GLA-BG were labeled with reducible biotin on ice and then incubated at 37°C (5–15 min) to induce internalization (Fig. 6, D and E). After stripping the remaining surface biotin by reduction, cell lysates were prepared, and internalized TfR was detected by immunoblotting streptavidin (SA)-bound proteins. Whereas mock-treated cells showed an increase in internal TfR (SA bound), BG-GLA-BG–treated cells did not. Additionally, surface levels of TfR on the BG-GLA-BG–treated cells were lower at the start of the internalization experiment, reflecting endosomal trapping of TfR that was occurring during the 2 h of cross-linker treatment before biotinylation. Together, analysis of transferrin and TfR traffic showed that BG-GLA-BG treatment of clone 3.3 is effective for acute inactivation of clathrin function in receptor-mediated endocytosis and shares phenotypic effects with other acute clathrin inactivation methods (Moskowitz et al., 2003; Deborde et al., 2008).

Inactivation of CHC17 during S phase induces centrosome fragmentation at metaphase

To acutely inactivate CHC17 function at specific points during the cell cycle, HeLa-SNAP-uLCa cells were enriched to S phase by double thymidine block (T/T; Fig. 7 A). Cell cycle synchronization was confirmed by propidium iodide labeling of DNA and flow cytometry, which revealed that cells were enriched to the G2/M phase between 7 and 8 h after release from the second thymidine block. Synchronized cells were then treated with BG-GLA-BG immediately after the block was released just before mitotic entry (T_0; Fig. 7 A) or treated with BG-GLA-BG 7 h after T/T at the time of metaphase onset (T_7; Fig. 7 A) or mock treated at these times. These were 2-h treatments and therefore extended 0–2 and 7–9 h after T/T for T_0 and T_7, respectively. Cell lysates were prepared during the post-T/T period, and comparable levels of covalent dimers of SNAP-uLCa were detected between 2 and 12 h after T_0 treatment and at 12 h after T_7 treatment (Fig. 7 B). Thus, SNAP-tag–mediated cross-linking is effective in synchronized cells. We further examined the levels for CHC and CLC isoforms in cells treated at T_0 and harvested 2–12 h after T/T, and these were unchanged when comparing BG-GLA-BG and mock treatments (Fig. S3, A and B).

The T_0 treatment with BG-GLA-BG made it possible to assess whether the centrosome amplification and multipolar spindles that occur upon CHC17 depletion (Figs. 1 and 2) are an immediate or long-term effect of losing clathrin function. Examination of cells 2 h after BG-GLA-BG treatment (4 h, after T_0) showed no obvious change in centrosome morphology (Fig. 7 C). However, by early mitosis (8 h, after T_0), fragmented centrosomes were observed (Fig. 7 D) as well as multipolar spindles (Fig. S3 C). Quantification of early mitotic cells with fragmented centrosomes confirmed the significance of this observation (Fig. 7 E). Analysis of γ-tubulin distribution relative to the central point of spindle pole–associated centrosomes (Fig. 7 F) revealed significant dispersion of the γ-tubulin signal in BG-GLA-BG–treated prometaphase cells. In contrast to clathrin depletion by siRNA, acute CHC17 inactivation produced only marginal increases in multinucleated cells after T_0 and T_7 BG-GLA-BG treatments when compared with mock treatments (Fig. S3 D). Thus, although

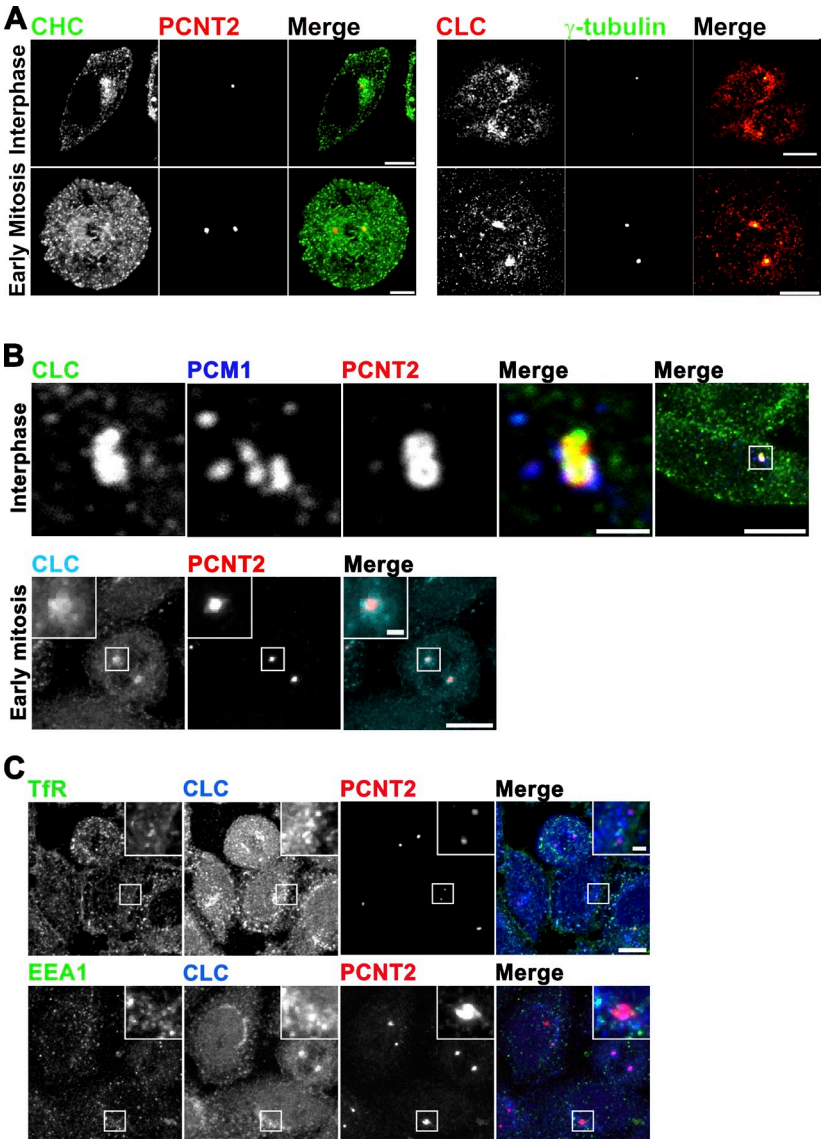

Figure 5. **Clathrin localizes at centrosomes of interphase and metaphase cells.** (A) HeLa cells were methanol fixed and processed for IF to detect CHC (X22 mAb) or CLC (rabbit polyclonal) and centrosomal markers PCNT2 (goat polyclonal) and γ-tubulin (mAb) at indicated cell cycle phases. Colocalization of green and red is shown as yellow. Bars, 10 µm. (B) HeLa-SNAP-uLCa clone 3.3 cells were methanol fixed and processed for IF to detect LCa with mAb X16 (CLC), PCM1 (rabbit polyclonal), and PCNT2 (goat polyclonal). Merged colors showing colocalization between labeled proteins are shown as yellow (red and green) and white (red, green, and yellow or cyan and red). Bars: (top) 2 µm; (bottom) 10 µm. (C) HeLa-SNAP-uLCa clone 3.3 cells were methanol fixed and processed for IF to detect TfR (mAb) or EEA1 (mAb), CLC with polyclonal rabbit antibody, and PCNT2 (goat polyclonal). Merged colors showing colocalization between CLC and PCNT2 are shown as pink. Bar, 10 µm. (A–C, insets) Boxes in each frame are magnified threefold. Bars, 2 µm. Images shown are 3D maximum projections.

acute inactivation of CHC17 at T_0 during S phase affects centrosome integrity during early mitosis, a significant multinuclear phenotype is not an immediate consequence of clathrin inactivation during this period. Notably, multinucleation was observed even less after clathrin inactivation later in the cell cycle at T_7, suggesting that the multinucleation that occurs after siRNA depletion of clathrin (Fig. 4) reflects compounded effects over multiple cell cycles.

ch-TOG levels are reduced in early mitotic cells and at centrosomes as a consequence of clathrin inactivation at S phase

Aurora A protein levels and kinase activity peak at the onset of G2/M, and inhibition of its activity is documented to prevent centrosome separation, centrosome maturation, and bipolar spindle formation (Hannak et al., 2001; Berdnik and Knoblich, 2002; Marumoto et al., 2003; Mori et al., 2007; Sardon et al., 2008). The centrosome phenotype induced by treating clone 3.3 cells in S phase with BG-GLA-BG was comparable with defects caused by treatment of cells with the Aurora A kinase inhibitor MLN8054, with respect to frequency of centrosome fragmentation and changes in γ-tubulin distribution (Fig. 7, D–F). Aurora A kinase activity is also required for formation of a complex between CHC17 clathrin, TACC3, and ch-TOG at the mitotic spindle, which stabilizes kinetochore microtubules (Fu et al., 2010; Lin et al., 2010; Booth et al., 2011; Cheeseman et al., 2011). During mitosis, both TACC3 and ch-TOG proteins are largely concentrated at centrosomes (Charrasse et al., 1998; Gergely et al., 2000) and spindles and are established to function in centrosome maturation and spindle pole formation as well as spindle stability (Gergely et al., 2003; Cassimeris and Morabito, 2004). Therefore, we investigated whether TACC3 and ch-TOG were present with clathrin at the centrosome in interphase cells (Fig. 8) and found that all three components were colocalized. Colocalization was not dramatically affected after 2 h of BG-GLA-BG treatment, though the CLC signal at the centrosome was reduced by cross-linking (Fig. 8, A and B). However, by 8 h into the cell cycle (6 h after cross-linking in S phase), ch-TOG protein levels were reduced about twofold compared with mock-treated cells (Fig. 8, C and E). As cells progress to mitosis, both

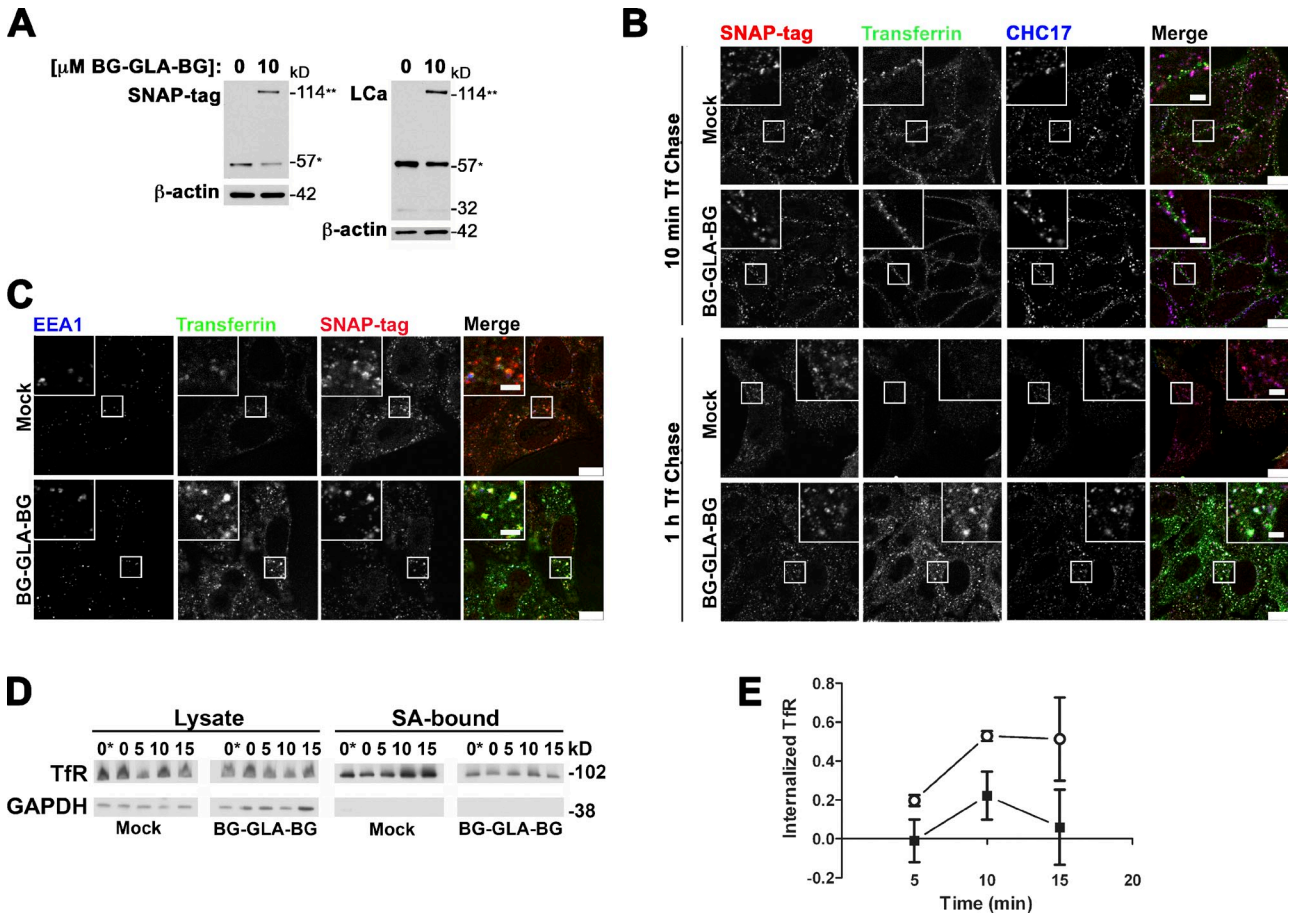

Figure 6. **Covalent cross-linking of SNAP-uLCa disrupts CHC17-dependent pathways of transferrin uptake and recycling.** (A) HeLa-SNAP-uLCa clone 3.3 cells were treated with SNAP-tag homodimerizer (BG-GLA-BG, 10 µM) or mock treated (0 µM) with solvent (DMSO) equivalent to the amount used for the BG-GLA-BG treatment. Cell lysates were immunoblotted for dimerized SNAP-uLCa (114** kD), monomeric SNAP-uLCa (57* kD), and endogenous uLCa (32 kD) using antibodies to the SNAP-tag or LCa (mAb X16), as indicated (left). β-actin was detected as a loading control. Protein mass based on migration relative to marker proteins is shown on the right. (B) Clone 3.3 cells were treated (2 h) with 5 µM BG-GLA-BG or equivalent DMSO (mock). Internalization of prebound (4°C) Alexa Fluor 488–transferrin (Tf) was visualized after 10 min or 1 h at 37°C after IF labeling with antibodies to the SNAP-tag or CHC17. Red-blue colocalization in merge is pink. Three-color colocalization in merge is white. Bars, 10 µm. (C) Clone 3.3 cells internalized prebound Alexa Fluor 488–transferrin for 1 h and were labeled by IF with antibodies to the SNAP-tag and EEA1. Red-green colocalization in merge is yellow. Three-color colocalization in merge is white. Bars, 10 µm. (B and C, insets) Boxes are magnified threefold. Bars, 1 µm. Images are 2D. (D) Clone 3.3 cells were treated with BG-GLA-BG or DMSO (mock), as in B, labeled with NHS-S-S-biotin, and then kept on ice (0* and 0 min) or incubated at 37°C for 5, 10, or 15 min. After reduction (stripping) of all samples except 0*, cells were lysed and analyzed by immunoblotting for total TfR and GAPDH (lysate), or biotinylated proteins were SA bound and immunoblotted to detect internalized TfR or control GAPDH. Protein mass based on migration relative to marker proteins is shown on the right. (E) TfR uptake (signal at internalization time point minus signal at time 0) was quantified by densitometry and plotted relative to total biotinylated TfR (0* minus signal at time 0) for four independent experiments, performed as in D for clone 3.3 cells treated with BG-GLA-BG (shaded squares) or DMSO (mock; open circles). Internalized TfR is shown in arbitrary units. Data represent the mean ± SEM of three separate experiments.

TACC3 and ch-TOG proteins are known to steadily increase and peak at mitotic onset (Gergely et al., 2003). This increase was not observed for ch-TOG after clathrin inactivation, whereas TACC3 levels were not significantly affected (Fig. 8, C–E).

Consistent with a reduction in overall ch-TOG levels, IF analysis showed that ch-TOG was partially reduced at metaphase centrosomes 6 h after clathrin cross-linking in S phase (Fig. 9). Clathrin itself was also reduced at the centrosome 2 h after and 6 h after S-phase treatment with cross-linker (Figs. 7 C and 9 A), suggesting that clathrin association with the centrosome must be dynamic, as confirmed by live imaging studies described in the next section. Again, the morphological effects of acute clathrin inactivation in S phase were mimicked by treatment of cells with Aurora A kinase inhibitor MLN8054, which caused a reduction of clathrin and ch-TOG at the early mitotic centrosome (Fig. 9). This further suggests that formation of the Aurora A–dependent clathrin–TACC3–ch-TOG complex contributes to centrosomal localization of these components. FACS analysis indicated that the timing of cell cycle entry was not affected by clathrin inactivation in S phase (Fig. S4), though effects on centrosomes and ch-TOG levels were observed early in mitosis (Figs. 7–9). This suggests that clathrin inactivation affects centrosome integrity just after G2/M onset, a period in which centrosome maturation occurs.

Live-cell imaging of clathrin and pericentrin reveals a dynamic and common route for centrosomal targeting

An advantage to the SNAP-tag is that it can be visualized in live cells using SNAP-TMR-Star. Clone 3.3 was transiently

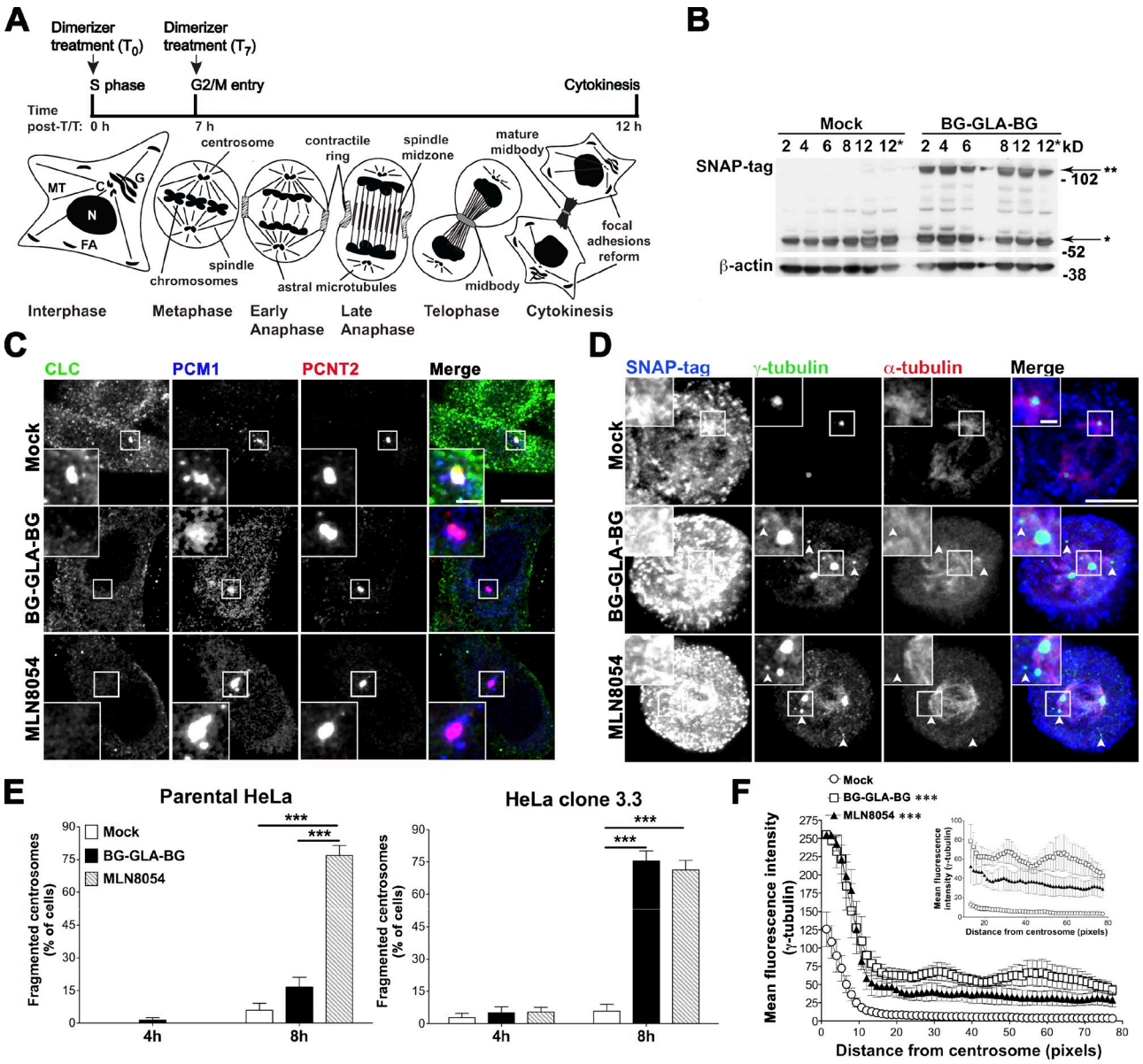

Figure 7. **Acute inactivation of clathrin during S phase causes centrosome fragmentation in early mitosis.** (A) To inactivate clathrin at specific times during the cell cycle, cells expressing the SNAP-uLCa were enriched in S phase by T/T and treated (2 h) with BG-GLA-BG immediately (T_0) upon thymidine washout (0–2 h after T/T) or at 7 h (T_7; 7–9 h after T/T). The timing of treatment relative to cell cycle phase is shown, as empirically determined for the transfected HeLa clones in this study. Corresponding cellular events are illustrated with the nucleus (N), microtubule networks (MT), Golgi (G), centrosomes (C), and focal adhesion structures (FA) indicated. (B) Clone 3.3 cells were enriched to S phase and then treated (2 h) with 5 µM BG-GLA-BG or mock treated, starting at T_0 or T_7 after T/T. Lysates prepared 2, 4, 6, 8, and 12 h after T/T for the T_0 treatment and at 12 h after T/T (12*) for the T_7 treatment were immunoblotted with antibodies to the SNAP-tag or β-actin (loading control). Migration positions of the SNAP-uLCa dimer (**), monomer (*), and molecular mass marker proteins are shown on the right. (C) Clone 3.3 cells were enriched to S phase by T/T block, and, at T_0, cells were treated with BG-GLA-BG (10 µM for 2 h), MLN8054 (500 nM for 4 h), or DMSO (mock; 4 h). 4 h after T_0, cells were methanol fixed and processed for IF to detect CLC (X16), PCM1, and PCNT2. Red-blue localization is pink in merge, and three-color localization is white. Bar, 10 µm. (D) Clone 3.3 cells were enriched to S phase by T/T block, and then, at T_0, cells were treated with BG-GLA-BG (10 µM for 2 h), MLN8054 (500 nM for 8 h), or DMSO (mock; 8 h). As cells entered mitosis (8 h after T_0), they were fixed with PFA and processed for IF to detect the SNAP-tag, γ-tubulin, and α-tubulin. Red-blue localization is pink in merge, and green-blue localization is cyan. Bar, 10 µm. (C and D, insets) Boxed regions are magnified threefold. Bars, 2 µm. Images are 3D maximum projections. (E) Clone 3.3 cells were enriched to S phase by T/T block, and, at T_0, cells were treated with BG-GLA-BG (10 µM for 2 h), MLN8054 (500 nM for 4 or 8 h), or DMSO (mock; 4 or 8 h, as in C and D). Treated cells were processed for IF to detect γ-tubulin and α-tubulin and were scored for centrosome fragmentation (γ-tubulin fragments shown by arrowheads in D). Data represent the mean ± SEM of two separate experiments (***, $P < 0.001$). 70 cells were scored per experiment. (F) From the experiment in D, 3D maximum projections of images of prometaphase and metaphase cells were analyzed for the distribution of γ-tubulin at the spindle pole–associated centrosome using the Radial Profile Extended plug-in in ImageJ. The normalized, integrated fluorescence intensity (y axis) is compared with the distance (pixels) of detected γ-tubulin at and surrounding the centrosome for cells treated with BG-GLA-BG, MLN8054, or DMSO (mock). The inset graph shows a magnified portion of the main graph and highlights the γ-tubulin fragments detected further out from the spindle pole–associated centrosome. Data represent the mean ± SEM of two to five prometaphase or metaphase cells (***, $P < 0.001$).

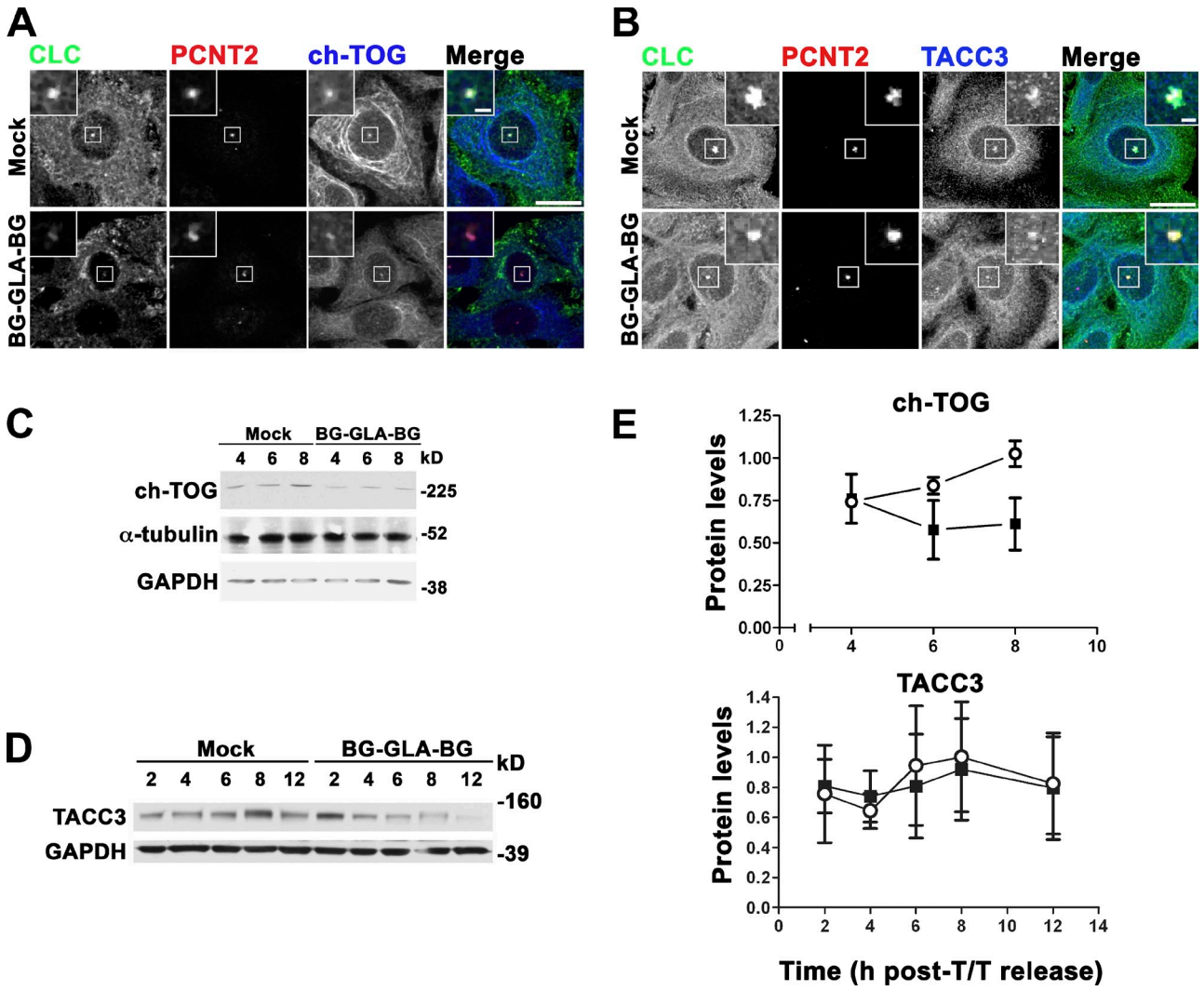

Figure 8. **Clathrin colocalizes with TACC3 and ch-TOG at interphase centrosomes, and ch-TOG levels are reduced by clathrin inactivation at S phase.** (A) Asynchronous clone 3.3 cells were treated (2 h) with 5 µM BG-GLA-BG or DMSO (mock) and then methanol fixed and processed for IF to detect LCa (mAb X16), PCNT2, and ch-TOG. Three-color colocalization is white in the merged image, and red-blue colocalization is pink. Bar, 10 µm. (B) Asynchronous clone 3.3 cells were treated as in A, methanol fixed, and then processed for IF to detect LCa (rabbit polyclonal), PCNT2, and TACC3. Three-color colocalization is white in the merged image. Bar, 10 µm. (A and B, insets) Boxed regions are magnified threefold. Bars, 1 µm. Images are 3D maximum projections. (C) Clone 3.3 cells were enriched to S phase by T/T block and treated (2 h) at T_0 with BG-GLA-BG or mock treated, as in A. Lysates prepared 4, 6, and 8 h after T/T were immunoblotted to detect ch-TOG, α-tubulin, and GAPDH, as indicated. Molecular mass marker position is shown on the right. (D) Clone 3.3 cells were enriched to S phase and treated with BG-GLA-BG or DMSO, as in C. Lysates prepared 2, 4, 6, 8, and 12 h after T/T were immunoblotted to detect TACC3 and GAPDH, as indicated. The immunoblot shown here comes from the same transfer membrane used to generate the immunoblot in Fig. S3 A. The transfer membrane was cut into horizontal strips of different molecular mass zones to detect all proteins shown here and in Fig. S3 A. Molecular mass marker position is shown on the right. (E) The densitometric quantification of immunoblots from multiple experiments performed as in C and D for clone 3.3 cells treated with BG-GLA-BG (shaded squares) or mock treated (open circles) relative to the loading control GAPDH. Data represent the mean ± SD of three to four separate experiments.

transfected to express GFP-pericentrin to perform comparative live-cell imaging of clathrin and pericentrin in the vicinity of the centrosome. Pericentrin is a constant resident of interphase and mitotic centrosomes in somatic cells and is known to be a key player in centrosome and spindle organization (Doxsey et al., 1994; Dictenberg et al., 1998). Additionally, pericentrin has been shown to traffic to the centrosome via pericentriolar satellite vesicles along microtubules (Young et al., 2000). Time-lapse confocal microscopy (at 37°C with 5% CO_2) was performed for live-cell imaging of CHC17 clathrin with SNAP-uLCa bound by SNAP-TMR-Star and the expressed GFP-pericentrin (48 h). Clathrin was constitutively colocalized with GFP-pericentrin at interphase and mitotic centrosomes (Fig. 10 A). In addition, vesicle-like structures that were positive for both SNAP-TMR-Star–labeled clathrin and GFP-pericentrin were observed in the vicinity of centrosomes (Fig. 10 [A and B] and Video 1), with the distribution of previously described pericentriolar satellites. By magnification of events at a late-interphase centrosome and performing time-lapse imaging with shorter scanning intervals, it was possible to visualize satellite structures colabeled for GFP-pericentrin and clathrin that were moving toward centrosomes (Fig. 10 C and Video 2). These time-lapse images indicate that clathrin localizes to centrosomes using a dynamic pathway that is shared by pericentrin and that their

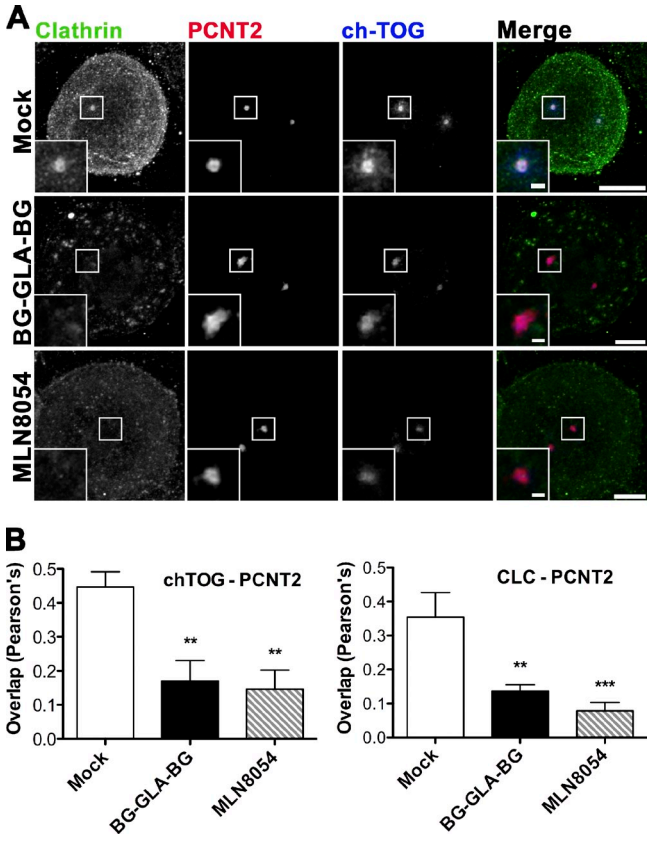

Figure 9. **Clathrin inactivation or inhibition of Aurora A kinase reduces clathrin and ch-TOG at centrosomes.** (A) Clone 3.3 cells were synchronized by T/T block and treated at T_0 with BG-GLA-BG for 2 h or the Aurora A kinase inhibitor MLN8054 for 8 h. 8 h after T_0, cells were fixed in methanol and processed for IF to visualize clathrin (mAb X16), PCNT2, and ch-TOG. Three-color colocalization in merge is white, and red-blue colocalization in merge is pink. Bars, 5 µm. (insets) Boxed regions are magnified. Bars, 2 µm. (B) Quantification by Pearson's coefficient of overlap between the centrosomal marker PCNT2 and clathrin or ch-TOG for each treatment in A. Data represent the mean ± SEM from two independent experiments (**, $P < 0.01$; ***, $P < 0.001$).

colocalization persists throughout the cell cycle. The data further suggest that clathrin recruitment to the centrosome coincides with a known centrosome maturation pathway (Telzer and Rosenbaum, 1979; Kuriyama and Borisy, 1981; Nigg and Raff, 2009).

Discussion

In this study, we identify a novel role for CHC17, and not CHC22 clathrin, in centrosome maturation. Clathrin isoform roles were distinguished and defined by a combination of RNAi depletion of clathrin isoforms and acute inactivation of CHC17 using chemical cross-linking. Inactivation of CHC17 in S phase resulted in centrosome fragmentation during the ensuing early mitosis as well as an increase in amplified centrosomes and multipolar spindles. These observations recapitulated centrosome amplification induced by RNAi depletion of CHC17 and indicated direct participation of CHC17 in centrosome maturation. This defines a new cell cycle role for CHC17 in addition to its recent implications in mitotic spindle stability (Fu et al., 2010; Lin et al., 2010; Booth et al., 2011) and in endosomal transport during cytokinesis (Thompson et al., 2002; Schweitzer et al., 2005; Prekeris and Gould, 2008; Joshi et al., 2010). Furthermore, these observations explain previous reports that perturbation of clathrin-associated proteins caused centrosomal defects (Thompson et al., 2004; Lehtonen et al., 2008; Liu and Zheng, 2009; Shimizu et al., 2009). In contrast, depletion of the CHC22 clathrin isoform by RNAi did not induce centrosome amplification, though its depletion did generate a multinuclear phenotype comparable with that observed for CHC17 depletion, suggesting that CHC22 contributes to cell division by a distinct mechanism.

To investigate clathrin function within the time frame of a single cell cycle and thereby address roles for clathrin at specific stages, we used a new approach to acute inactivation of clathrin function. In our hands, the SNAP-tag modification we adopted (Lemercier et al., 2007) was more effective at clathrin inactivation than the FK506-binding protein modification (Moskowitz et al., 2003), Killer red modification (Bulina et al., 2006), or the CALI (chromophore-assisted light inactivation) modification (Heerssen et al., 2008), the latter being plagued by background binding of the light-sensitive Lumio compound (unpublished data). The SNAP-tag was also useful for binding fluorescent dye as well as cross-linker (Juillerat et al., 2003; Lemercier et al., 2007). The cross-linking approach to inactivation has the advantage of targeting clathrin itself, rather than interfering with clathrin–adaptor interactions like the recently developed pitstop chemical inhibitors of clathrin function (von Kleist et al., 2011). Although useful, the pitstops may be limited to affecting trafficking functions of clathrin in cells and may not probe clathrin interactions that do not depend on binding the clathrin box of adaptors that they target.

Acute inactivation of CHC17 clathrin in S phase using the BG-GLA-BG cross-linker bound to SNAP-tagged CLC produced a fragmented centrosome phenotype in early mitosis but had no effect on cell cycle entry. Cross-linker treatment in S phase also reduced the presence of clathrin at mitotic centrosomes and reduced whole-cell levels of ch-TOG as well as its levels at mitotic centrosomes. These observations suggest that clathrin contributes to stability of the ch-TOG protein early in the cell cycle. This effect on ch-TOG and the fact that clathrin inactivation can be phenocopied by inhibition of Aurora A kinase suggests that clathrin's role in centrosome maturation involves its participation in a complex with TACC3 and ch-TOG, which has been shown to form upon Aurora A kinase phosphorylation of TACC3. This complex has so far been characterized at the mitotic spindle (Royle, 2012) as contributing to the stability of kinetochore microtubules. Here, we provide evidence of all three components at the interphase centrosome as well and propose that the low level of Aurora A activity before G2/M onset could initiate centrosomal formation of the complex. We further propose that the clathrin–TACC3–ch-TOG complex could contribute to the stability of centrosomal tubulin because we show that centrosomal loss of complex components induces γ-tubulin dispersion and centrosome fragmentation. Interestingly, TACC3 localization at the centrosome and TACC3 cell cycle levels were not affected by clathrin inactivation, suggesting that TACC3 is the recruiting component for the complex,

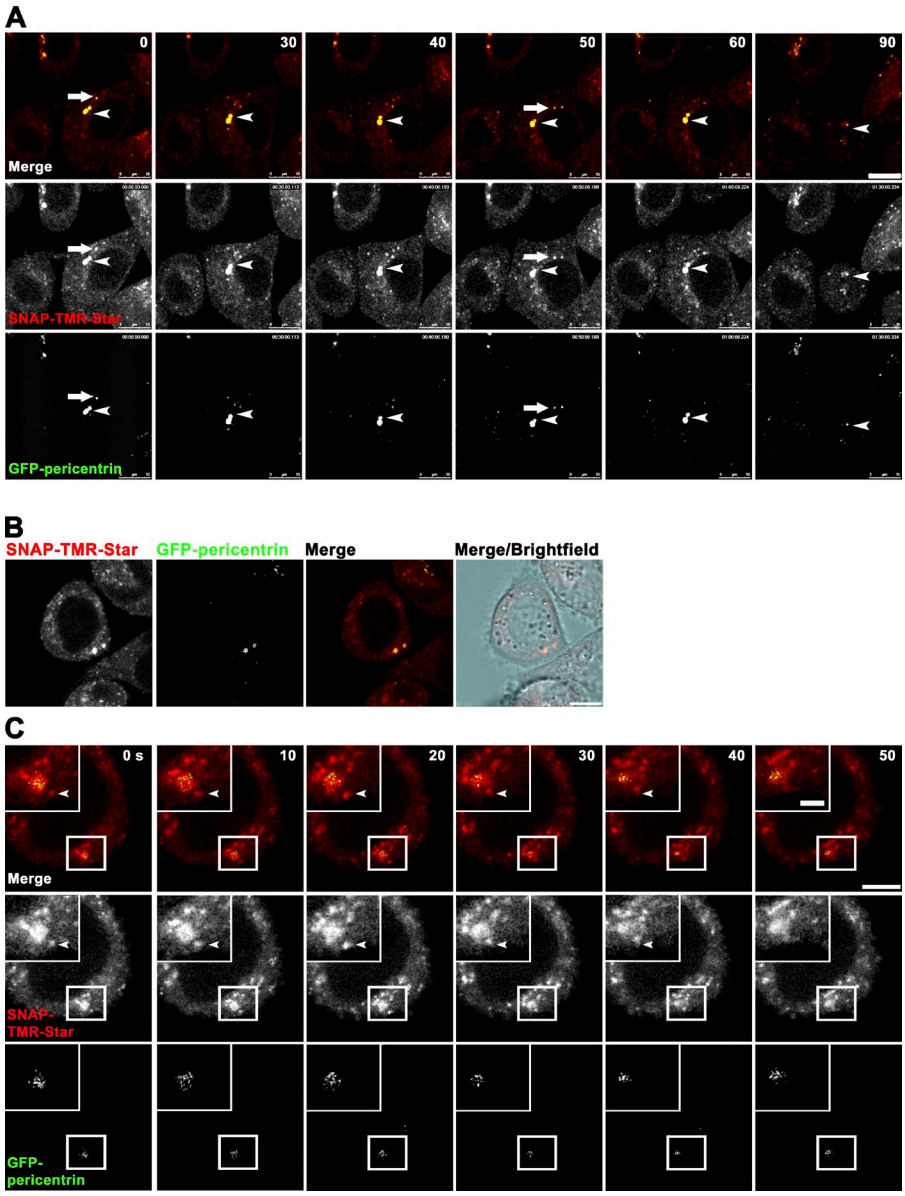

Figure 10. **Clathrin and pericentrin traffic along a shared route toward late-interphase centrosomes.** (A) Asynchronous clone 3.3 cells were transiently transfected with GFP-pericentrin 48 h before labeling SNAP-uLCa with SNAP-TMR-Star. Cells were analyzed over 2 h by time-lapse confocal microscopy, taking 2D images every 10 min (37°C in 5% CO_2 at 95% humidity). Colocalization (yellow in merged images) between SNAP-TMR-Star–labeled SNAP-uLCa and GFP-pericentrin occurs at centrosomes (arrowheads) and adjacent submicrometer vesicles (arrows). Top right corners of merged images show time interval in minutes. Bar, 10 µm. Images are 3D maximum projections. (B) Asynchronous clone 3.3 cells transiently transfected with GFP-pericentrin and labeled with SNAP-TMR-Star were imaged by confocal microscopy. Colocalization of pericentrin and SNAP-uLCa is shown (yellow in merged image) at two separated centrosomes of a late-interphase cell and overlayed with the brightfield image. Bar, 10 µm. Images are 2D. (C) The cell shown in B was magnified twofold and analyzed by time-lapse confocal microscopy for 2 min with 10-s imaging intervals. SNAP-uLCa localizes with GFP-pericentrin at the centrosome, and pericentriolar SNAP-uLCa vesicles move toward the centrosome (arrowheads). Top right corners of merged images show the time interval. Bars, 5 µm. (insets) Boxed regions are magnified threefold. Bars, 2 µm. Images are 3D maximal projections.

as has been suggested for clathrin recruitment to the mitotic spindle (Royle, 2012). Inhibition of Aurora A kinase would also prevent TACC3 from recruiting clathrin and ch-TOG, explaining the shared phenotype with clathrin inactivation.

Although our data are consistent with clathrin's centrosomal role involving its complexation with ch-TOG and TACC3, the possibility remains that clathrin also plays a membrane traffic function at the centrosome. Live-cell imaging shown here indicates that clathrin and pericentrin take the same route to the centrosome. The simplest interpretation of this data is that they both traffic along microtubules, a known pathway for delivering components to the maturing centrosome (Young et al., 2000). However, it is possible that clathrin-coated vesicles could serve as vehicles for delivering other centrosomal components in addition to clathrin itself. In light of this possibility, it is interesting that depletion of the clathrin adaptors ARH or epsin affects centrosome integrity (Lehtonen et al., 2008; Liu and Zheng, 2009). As adaptors link cargo to a clathrin-coated vesicle, their depletion is most likely to affect membrane traffic. In contrast, the other clathrin-associated protein, whose depletion causes centrosomal defects, is GAK, which plays a role in the clathrin-uncoating cycle (Shimizu et al., 2009). GAK loss could cause clathrin sequestration and thereby affect complexation with ch-TOG and TACC3.

Defects in all of the defined functions of CHC17 during the cell cycle could result in multinucleation. We observed that inactivation of CHC17 during S phase and at a later stage of mitosis resulted in considerably less multinucleation in one cell cycle than seen after 48–72 h of RNAi depletion of CHC17. Thus, the phenotype of multinucleation arises after cumulative loss of CHC17 functions during multiple rounds of mitosis. CHC22 depletion by RNAi resulted in an increase in multinucleated cells comparable with that induced by CHC17 depletion (Fig. 4). As CHC22 depletion did not affect centrosome number or maturation (Figs. 1 and 2) and endogenously expressed CHC22 does not associate with the mitotic spindle (Esk et al., 2010), it may influence later phases in mitosis that affect cytokinesis. A likely

possibility is that CHC22's distinct role in endosomal sorting (Esk et al., 2010) contributes to the extensive endosomal membrane traffic involved in midbody abscission (Montagnac et al., 2008; Prekeris and Gould, 2008) and that multinucleation arises from interfering with CHC22's role in this traffic.

In summary, this study takes advantage of acute CHC17 clathrin inactivation within the cell cycle and complements prior studies involving lengthy RNAi treatment or deletion mutation. Considering all studies together suggests there are at least three temporally distinct processes by which clathrin function regulates mitotic progression. These are centrosome maturation (shown here), mitotic spindle stability (Royle et al., 2005; Royle and Lagnado, 2006; Lin et al., 2010), and cytokinesis (Niswonger and O'Halloran, 1997; Schweitzer et al., 2005). Here, we demonstrate that centrosome maturation requires CHC17 clathrin and that CHC22 clathrin influences the cell cycle independently, further establishing that functions of both clathrins are required for normal cell division.

Materials and methods

Antibodies

Primary antibody concentrations ranged from 1–5 µg/ml for immunoblotting and IF assays. Antibodies specific for clathrin isoforms produced in our laboratory include mAb TD.1 against CHC17 (Näthke et al., 1992), mAb X22 against CHC17 (Brodsky, 1985a), rabbit pAb against CHC22 (Vassilopoulos et al., 2009), rabbit pAb against both CLCs (Acton et al., 1993), and mAb X16 against LCa (Brodsky, 1985a). A rabbit pAb against ch-TOG used for IF assays exclusively was a gift from L. Cassimeris (Lehigh University, Bethlehem, PA). Commercially available antibodies were used to detect β-actin (mAb; Sigma-Aldrich), γ-tubulin (mAb; Santa Cruz Biotechnology, Inc.), α-tubulin (mAb from Sigma-Aldrich and rabbit polyclonal from Santa Cruz Biotechnology, Inc.), PCNT2 (goat polyclonal; Santa Cruz Biotechnology, Inc.), centrin-2 (mAb; Abcam), SNAP-tag (rabbit polyclonals from both GenScript and New England Biolabs, Inc.), TACC3 (mAb; Santa Cruz Biotechnology, Inc.), ch-TOG (rabbit polyclonal from AbCam and rabbit polyclonal from BioLegend), PCM1 (rabbit polyclonal; Cell Signaling Technology), glyceraldehyde 3-phosphate dehydrogenase (GAPDH; mAb; EMD Millipore), TfR (mAb; BD), and EEA1 (mAb; BD). Immunoblotting studies used secondary antibodies conjugated to HRP (Invitrogen) at 1:10,000 or 1:20,000. Secondary antibodies for IF included Alexa Fluor antibody conjugates 488, 555, and 647 (Molecular Probes or Invitrogen) and were used at 1:400 or 1:500.

Plasmids

The cDNA encoding nonneuronal human uLCa was cloned into plasmid DNA such that the SNAP-tag (New England Biolabs, Inc.) was incorporated at the N-terminal end of uLCa. The cDNA vector for GFP-pericentrin (pLPx7-GFP-pericentrin) was produced in the Doxsey laboratory at the University of Massachusetts Medical School.

Cell culture and siRNA transfection

HeLa cells stably expressing either GFP–α-tubulin or centrin-2–GFP were gifts from A. Straight (Stanford University, Stanford, CA) and M.-F.B. Tsou (Sloan-Kettering Institute, New York, NY), respectively. These cells were maintained in DME (Invitrogen) supplemented with 10% FBS, 100 U/ml penicillin, 100 µg/ml streptomycin, 10 mM Hepes, and 500 µg/ml G418 (Corning). Normal HeLa cells were maintained using the same media without G418.

Duplex siRNAs were synthesized (QIAGEN) based on experimentally validated target sequences for clathrin isoforms and subunits (Huang et al., 2004; Vassilopoulos et al., 2009), γ-tubulin (Hs_TUBG1_5, catalog no. S102780750), or nonsilencing siRNA (catalog no. 1027310). For RNAi treatments, cells were seeded (21,000 cells/cm^2) in 6- or 24-well plates in Opti-MEM I reduced serum media (Invitrogen) and then transfected with duplex siRNAs (20 nM per treatment) complexed with HiPerFect (QIAGEN) in a 1:10 mixture (siRNA/HiPerFect). Conditions targeting CHC17 and CLCs together used a combination of 10 nM CHC17 and 10 nM CLC siRNA. CLC siRNA treatments included two parts siRNA-targeting LCa combined with one part siRNA-targeting LCb. CHC22 depletion was achieved by combining two siRNAs (1:1), as previously described (Vassilopoulos et al., 2009). 6 h after siRNA transfection, cells were returned to normal growth conditions and then harvested for analysis 48 to 72 h later. Targeting and nontargeting siRNA effects were confirmed by immunoblotting.

Generation of stable SNAP-uLCa HeLa cell clones

HeLa cells were seeded (50,000 cells/cm^2) in 6-well plates 1 d before plasmid transfection (5 h at 37°C in 5% CO_2) using Lipofectamine 2000 (2.0 µg plasmid in 5 µl Lipofectamine 2000) and Opti-MEM I reduced serum media according to the manufacturer's instructions (Invitrogen). For 48 h after transfection, cells were cultured under nonselective conditions, and then they were passaged in DME supplemented with 10% FBS, 10 mM Hepes, 100 U/ml penicillin, 100 µg/ml streptomycin, and 700 µg/ml G418 (G418 selection media). Single colonies were selected 1.5–2 wk after adding G418 selection media. Sterile glass cylinders (Thermo Fisher Scientific) were stamped in autoclaved vacuum grease (Corning) to trypsinize single resistant colonies for expansion. Clonal cell expression SNAP-uLCa was validated by immunoblotting, IF, and IP.

IF and confocal imaging

IF protocols were modified from established methods (Piehl and Cassimeris, 2003; Straight et al., 2005). Cells grown on a 0.17-mm coverglass (Corning) were fixed with 4% PFA (Electron Microscopy Sciences) diluted in cytoskeleton stabilization buffer (10 mM MES, pH 6.1, 138 mM KCl, 3 mM MgCl, and 2 mM EGTA) for 20 min at room temperature. Fixation was quenched with 25 mM glycine in PBS. To detect TACC3, ch-TOG, and clathrin at centrosomes, cells were fixed in −20°C methanol with 1 mM EDTA (10 min at room temperature; Piehl and Cassimeris, 2003). All fixed cells were permeabilized (10 min at room temperature) with TBS containing 0.5% Triton X-100, pH 7.4, washed two times with TBS–0.1% Triton X-100, pH 7.4, and blocked in antibody dilution buffer (Abdil; TBS containing 0.1% Triton X-100 and 2% wt/vol BSA, pH 7.4, for 10 min at room temperature). Primary antibodies (1–5 µg/ml in Abdil) were applied (2 h at room temperature), and, after washing with TBS containing 0.1% Triton X-100, Alexa Fluor secondary antibodies suspended in Abdil were applied (45 min at room temperature). Cells were then washed in TBS containing 0.1% Triton X-100 followed by TBS alone. Where indicated, cells were incubated with 300 nM DAPI to stain DNA (10 min at room temperature) and then washed in TBS. Cells were mounted for microscopy in 2.5% DABCO (Sigma-Aldrich), 50 mM TBS, pH 8.0, and 90% glycerol.

Cells processed by IF were analyzed by confocal laser-scanning microscopy using an inverted system (DM1 6000 CS, SP5; Leica) with oil immersion objectives (63× 1.4 NA and 100× 1.4 NA; both HCX Plan Apochromat; Leica) and argon (488) and HeNe (543 and 633) lasers. Images were acquired using LAS AF SP5 software (Leica) in sequential scan mode with a 600-Hz scan rate, line averages of four to six, and a 512 × 512– or 1,024 × 1,024–pixel resolution. Raw images were processed using LAS AF SP5, ImageJ (version 1.45c; National Institutes of Health), and Photoshop (CS3; Adobe). To improve image quality, raw images were processed using a median filter (LAS AF SP5) before any analysis was performed. Colocalization measurements were performed using LAS AF SP5, and fluorescence distribution measurements were performed on maximum projections of 3D images using the Radial Profile Extended plug-in (version 1, by Philippe Carl) in ImageJ (version 1.45c). Adjustments to brightness and contrast of images were restricted to the dynamic range of the fluorescent intensity profile for merged fluorophores, applied to the whole image, and the same settings were maintained for all samples within an experiment.

Time-lapse confocal microscopy imaging

Asynchronous cells were seeded (50,000 cells/cm^2) in 35-mm culture dishes 1 d before transfection with the GFP-pericentrin–encoding plasmid pLPx7-GFP-pericentrin using Lipofectamine 2000 (0.8-µg plasmid in 2 µl Lipofectamine 2000) and Opti-MEM I reduced serum media according to manufacturer's instructions. After transfection, the Opti-MEM I transfection media was removed, and cells were cultured in DME media supplemented with 10% FBS, 100 U/ml penicillin, 100 µg/ml streptomycin, and 10 mM Hepes for 48 h. Cells were then labeled with SNAP-TMR-Star (3 µM in phenol red–free DME with 10% FBS) for 30 min at 37°C according to manufacturer's instructions (New England Biolabs, Inc.). Cells were then detached from culture dishes using PBS-based Cell Dissociation Buffer (Invitrogen), pelleted (1,000 *g* for 5 min), resuspended in phenol red–free DME with 10% FBS, and seeded in Lab-Tek II chambered coverglass

(0.17-mm glass thickness; Thermo Fisher Scientific). This transfer step avoided residual SNAP-TMR-Star sticking to the coverglass surface. Cells were incubated (37°C in 5% CO_2 with 95% humidity) for 5 h before initiating time-lapse imaging.

SNAP-TMR-Star–labeled cells transiently expressing GFP-pericentrin were analyzed by confocal laser-scanning microscopy using an inverted system (DM1 6000 CS, SP5) with photomultiplier tube detection, an incubation chamber (37°C in 5% CO_2), an oil immersion objective (63× 1.4 NA; HCX Plan Apochromat), and argon (488 laser power, 2%) and HeNe (543 laser power, 10%) lasers. Images were acquired using LAS AF SP5 in xyt-sequential scan mode (10-s or 10-min scanning intervals), a 700-Hz scan rate, line averages of two, and a 512 × 512–pixel resolution. Raw images were processed using a median filter in ImageJ (version 1.45c). Adjustments to brightness and contrast of images were performed in Photoshop (CS3), restricted to the dynamic range of the fluorescent intensity profile for merged fluorophores, and applied to the whole xyt image sequence series, and the same settings were maintained for all samples within an experiment.

Immunoblot analysis

Cell lysates were resolved by SDS-PAGE (NuPage Bis-Tris 4–12% SDS-acrylamide gels; Invitrogen), transferred to nitrocellulose membranes (EMD Millipore), and exposed to primary (1–5 µg/ml) and peroxidase-conjugated secondary antibodies. Labeled proteins were detected using the ECL-Plus reagent (GE Healthcare). Molecular mass markers (Rainbow; GE Healthcare) were used for calibration, and protein band intensities were quantified using Quantity One (Bio-Rad Laboratories) or ImageJ (version 1.45c) software. For detection of the SNAP-tag and CHC17 by blotting, the anti–SNAP-tag antibody (New England Biolabs, Inc.) and TD.1 antibody were used, respectively.

IP

The X22 mAb was used to immunoprecipitate CHC17 clathrin. IgG mAb (IgG1, κ; BD) was used as a control. IP was performed from cell lysate prepared in high-Tris IP lysis buffer (0.5 M Tris, pH 7.2, 1.0% Triton X-100, 20 mM EDTA, 5 µg/ml aprotinin, 10 µg/ml leupeptin, 10 µg/ml pepstatin A, and 1 mM PMSF), conditions that disassemble clathrin coats (Wilde and Brodsky, 1996). Lysates were diluted in IP lysis buffer to a standard concentration of 2 mg/ml and 100 µl used for each specific IP, first precleaning with protein G Sepharose (GE Healthcare), then incubating with 2 µg of primary antibody overnight at 4°C and then with protein G for 1 h at 4°C followed by washing (3×) with 500 µl of IP lysis buffer. Precleared and IP samples were resolved by SDS-PAGE, transferred to nitrocellulose membranes, and analyzed by immunoblotting.

SNAP-tag labeling, fusion protein cross-linking, and Aurora A kinase inhibition assays

For in vivo labeling of SNAP-tagged uLCa fusion proteins, live cells plated on coverslips were incubated (30 min at 37°C in 5% CO_2) with 3 µM SNAP-TMR-Star (New England Biolabs, Inc.) diluted in normal growth media with serum. Cells were then washed three times with normal growth media with serum, incubated (37°C in 5% CO_2) an additional 30 min, and then imaged using confocal laser-scanning microscopy, as detailed under Time-lapse confocal microscopy imaging.

Covalent cross-linking of SNAP-uLCa was achieved using BG-GLA-BG, a SNAP-tag homodimerizer shown in Fig. S5, synthesized at New England Biolabs, Inc. following established methods (Lemercier et al., 2007). Stable HeLa-SNAP-uLCa clones were treated at specified concentrations (5–10 µM) with BG-GLA-BG dissolved in DMSO and then diluted in normal growth media with serum and incubated (2 h at 37°C in 5% CO_2).

For treatment with the Aurora A kinase inhibitor MLN8054 (Selleck Chemicals) and comparison with BG-GLA-BG treatment, HeLa-SNAP-uLCa clone 3.3 cells were synchronized to S phase by T/T and then treated at 0 h (T_0) after T/T with DMSO (mock) for 4 or 8 h, 10 µM BG-GLA-BG for 2 h, or 500 nM MLN8054 for 4 or 8 h. At 4 and 8 h, cells were fixed with methanol containing 1 mM EDTA (10 min) and processed for IF.

Fluorescent transferrin internalization assay

Cells that were incubated in the presence or absence of homodimerizer were placed on ice, washed three times with ice-cold HBSS (Invitrogen), and then exposed to 50 µg/ml Alexa Fluor 488–conjugated transferrin (Invitrogen) in HBSS (30–60 min at 4°C). After washing (four times with HBSS at 4°C), prewarmed HBSS was added to cells, and cells were incubated (37°C in 5% CO_2) for 10 min to 1 h to allow for transferrin internalization. Immediately after this incubation, the cells were fixed at room temperature with 4% PFA and processed for IF.

Cell surface biotinylation and TfR internalization assay

Cell surface biotin labeling and receptor internalization assays were modified from established methods (Blagoveshchenskaya et al., 2002). HeLa-SNAP-uLCa clone 3.3 cells were seeded in five 60-mm dishes (80,000 cells/cm^2) 1 d before treating them with 5 µM BG-GLA-BG or DMSO (mock) for 2 h at 37°C, 5% CO_2, and 95% humidity. Cells were washed on ice with ice-cold PBS, pH 8.0, and then treated with 10 mM sulfo-NHS-SS-biotin (Thermo Fisher Scientific) for 30 min at 4°C. Unreacted biotin was quenched by washing cells with ice-cold PBS, pH 7.2, containing 50 µM glycine. Two dishes representing 0 min (0*, one to not be stripped of biotin, and 0, to be stripped of biotin) were kept on ice while the other remaining three dishes were treated with prewarmed PBS containing Ca^{2+} and Mg^{2+} and placed in a cell incubator for 5–15 min at 37°C, and then the reaction was stopped with 5 mg/ml iodoacetamide on ice. Cell lysates were prepared in high-Tris IP lysis buffer after washing with ice-cold PBS and exposed to SA agarose resin (Thermo Fisher Scientific) for 1 h at 4°C to pull down internalized biotin-labeled receptors. SA-bound samples representing plasma membrane–associated (0 min) and internalized (5, 10, and 15 min) receptors were pelleted by centrifugation and then washed five times with 1% NP-40 in PBS. SA-bound samples and total cell lysate for all time points were immunoblotted for TfR and GAPDH. To quantify the extent of internalized TfR, blotting signals were assessed by densitometry, and values defined for all time points were expressed in arbitrary units using the following equation:

$$\mathrm{TfR}^{\mathrm{int}} = \frac{t^{37} - t^{0}}{t^{0*} - t^{0}}.$$

$\mathrm{TfR}^{\mathrm{int}}$ represents internalized SA-bound TfR, plotted in Fig. 6. The symbol t^{37} represents internalized SA-bound TfR from lysates of cells treated at 5, 10, or 15 min at 37°C. t^{0} represents residual biotin at the plasma membrane of cells that were kept on ice and then stripped of biotin before lysis. t^{0*} is plasma membrane–associated, SA-bound TfR from lysates of cells that were kept on ice and not stripped of biotin before lysis.

Cell synchronization

Cells were synchronized to the G1/S-phase boundary using the T/T method (Bello, 1969). HeLa clones were seeded (15,000 cells/cm^2) in 10-cm dishes 1 d before treatment with 2 mM thymidine in normal G418 selection media for 19 h. Cells were released from this first thymidine block by washing with PBS (two times) followed by incubation in G418 selection media without thymidine for 9 h. A second thymidine block was then performed for an additional 16 h before returning cells to G418 selection media without thymidine. Cell synchronization was confirmed by flow cytometry after labeling cells with propidium iodide (Fig. S4). Synchronized cells were used in cross-linking experiments at varying time intervals after the second thymidine release was initiated (2, 4, 6, 8, and 10 h).

Flow cytometry

Synchronized cells were harvested by trypsinization (0.05% trypsin-EDTA; Invitrogen), centrifuged, and washed two times with ice-cold PBS. Cell pellets were fixed by slowly adding 70% ethanol (chilled at −20°C) while vortexing and then stored at 4°C. On the day of flow cytometry analysis, fixed cells were pelleted and washed two times with ice-cold PBS to remove ethanol. The supernatant was removed, and pellets were left to dry to avoid ethanol contamination. Cell pellets were then resuspended in PBS containing 40 µg/ml propidium iodide and 40 µg/ml ribonuclease A and incubated in the dark for 30–60 min at 37°C. Cells were analyzed for DNA content using a flow cytometer (BD). Data were processed using FlowJo software (version 9.4.11; Tree Star) to determine the proportion of cells in each phase of the cell cycle (Kawamoto et al., 1979).

Statistical analysis

Data were statistically analyzed using GraphPad Prism software (GraphPad Software). For nonparametric data, statistical analyses were performed using a one-way analysis of variance Friedman's matched pairs test and the Dunn's multiple comparison post-hoc test (90% confidence interval). A regular one-way analysis of variance was performed for data that passed the normality test, D'Agostino–Pearson omnibus test, and the post-hoc test was Tukey's multiple comparison test (95% confidence interval).

Online supplemental material

Fig. S1 shows quantification of the knockdown effects of all siRNA sequences used in this study, demonstrating reproducible effects on different transfected

HeLa cell clones when compared with nonsilencing siRNA. Fig. S2 shows binding of the SNAP-uLCa fusion protein to CHC17 in HeLa-SNAP-uLCa clones and colocalization with endogenous CHC17 clathrin in cells representing all phases of the cell cycle. Figs. S3 and S4 show that acute inactivation of clathrin by SNAP-tag–mediated cross-linking in clone 3.3 cells did not significantly affect CHC17, CHC22, or CLC levels, appearance of multinuclear cells within one round of mitosis, or cell cycle progression but did induce a multipolar spindle phenotype within one cell cycle. Fig. S5 shows the chemical structure of BG-GLA-BG. Video 1 shows a live-cell image of clathrin colocalization with GFP-pericentrin at an interphase centrosome and in local vesicular structures at 10-min intervals over 2 h. Video 2 shows a live-cell image of colocalized clathrin and GFP-pericentrin in small structures moving toward the centrosome of a G2/M-phase–transitioning cell at 10-s intervals over 2 min. Online supplemental material is available at http://www.jcb.org/cgi/content/full/jcb.201205116/DC1.

We thank Rebecca Heald (University of California, Berkeley, Berkeley, CA) for support and advice, Aaron Straight for helpful discussion and for the stable HeLa-GFP–α-tubulin cell line, Meng-Fu Bryan Tsou for the stable HeLa–centrin-2–GFP cell line, and Lynne Cassimeris for her advice and the ch-TOG antibody. We also thank Brenda Baker (New England Biolabs, Inc.) for assistance with synthesis of BG-GLA-BG.

This work was supported by National Institutes of Health grants GM038093 to F.M. Brodsky and GM051994 to S.J. Doxsey, National Institutes of Health training grant NCI T32 CA09043 to A.B. Foraker, and an Arthritis Foundation postdoctoral fellowship to T.M. Evans.

Submitted: 5 December 2011
Accepted: 12 July 2012

References

Acton, S.L., D.H. Wong, P. Parham, F.M. Brodsky, and A.P. Jackson. 1993. Alteration of clathrin light chain expression by transfection and gene disruption. *Mol. Biol. Cell*. 4:647–660.

Azimzadeh, J., and M. Bornens. 2007. Structure and duplication of the centrosome. *J. Cell Sci.* 120:2139–2142. http://dx.doi.org/10.1242/jcs.005231

Bello, L.J. 1969. Studies on gene activity in synchronized culture of mammalian cells. *Biochim. Biophys. Acta*. 179:204–213. http://dx.doi.org/10.1016/0005-2787(69)90137-3

Bennett, E.M., S.X. Lin, M.C. Towler, F.R. Maxfield, and F.M. Brodsky. 2001. Clathrin hub expression affects early endosome distribution with minimal impact on receptor sorting and recycling. *Mol. Biol. Cell*. 12:2790–2799.

Berdnik, D., and J.A. Knoblich. 2002. *Drosophila* Aurora-A is required for centrosome maturation and actin-dependent asymmetric protein localization during mitosis. *Curr. Biol.* 12:640–647. http://dx.doi.org/10.1016/S0960-9822(02)00766-2

Blagoveshchenskaya, A.D., L. Thomas, S.F. Feliciangeli, C.H. Hung, and G. Thomas. 2002. HIV-1 Nef downregulates MHC-I by a PACS-1- and PI3K-regulated ARF6 endocytic pathway. *Cell*. 111:853–866. http://dx.doi.org/10.1016/S0092-8674(02)01162-5

Bonazzi, M., L. Vasudevan, A. Mallet, M. Sachse, A. Sartori, M.C. Prevost, A. Roberts, S.B. Taner, J.D. Wilbur, F.M. Brodsky, and P. Cossart. 2011. Clathrin phosphorylation is required for actin recruitment at sites of bacterial adhesion and internalization. *J. Cell Biol.* 195:525–536. http://dx.doi.org/10.1083/jcb.201105152

Booth, D.G., F.E. Hood, I.A. Prior, and S.J. Royle. 2011. A TACC3/ch-TOG/clathrin complex stabilises kinetochore fibres by inter-microtubule bridging. *EMBO J.* 30:906–919. http://dx.doi.org/10.1038/emboj.2011.15

Boucrot, E., and T. Kirchhausen. 2007. Endosomal recycling controls plasma membrane area during mitosis. *Proc. Natl. Acad. Sci. USA*. 104:7939–7944. http://dx.doi.org/10.1073/pnas.0702511104

Brodsky, F.M. 1985a. Clathrin structure characterized with monoclonal antibodies. I. Analysis of multiple antigenic sites. *J. Cell Biol.* 101:2047–2054. http://dx.doi.org/10.1083/jcb.101.6.2047

Brodsky, F.M. 1985b. Clathrin structure characterized with monoclonal antibodies. II. Identification of in vivo forms of clathrin. *J. Cell Biol.* 101:2055–2062. http://dx.doi.org/10.1083/jcb.101.6.2055

Brodsky, F.M., C.J. Galloway, G.S. Blank, A.P. Jackson, H.F. Seow, K. Drickamer, and P. Parham. 1987. Localization of clathrin light-chain sequences mediating heavy-chain binding and coated vesicle diversity. *Nature*. 326:203–205. http://dx.doi.org/10.1038/326203a0

Brodsky, F.M., C.Y. Chen, C. Knuehl, M.C. Towler, and D.E. Wakeham. 2001. Biological basket weaving: Formation and function of clathrin-coated vesicles. *Annu. Rev. Cell Dev. Biol.* 17:517–568. http://dx.doi.org/10.1146/annurev.cellbio.17.1.517

Bulina, M.E., K.A. Lukyanov, O.V. Britanova, D. Onichtchouk, S. Lukyanov, and D.M. Chudakov. 2006. Chromophore-assisted light inactivation (CALI) using the phototoxic fluorescent protein KillerRed. *Nat. Protoc.* 1:947–953. http://dx.doi.org/10.1038/nprot.2006.89

Cassimeris, L., and J. Morabito. 2004. TOGp, the human homolog of XMAP215/Dis1, is required for centrosome integrity, spindle pole organization, and bipolar spindle assembly. *Mol. Biol. Cell*. 15:1580–1590. http://dx.doi.org/10.1091/mbc.E03-07-0544

Charrasse, S., M. Schroeder, C. Gauthier-Rouviere, F. Ango, L. Cassimeris, D.L. Gard, and C. Larroque. 1998. The TOGp protein is a new human microtubule-associated protein homologous to the *Xenopus* XMAP215. *J. Cell Sci.* 111:1371–1383.

Cheeseman, L.P., D.G. Booth, F.E. Hood, I.A. Prior, and S.J. Royle. 2011. Aurora A kinase activity is required for localization of TACC3/ch-TOG/clathrin inter-microtubule bridges. *Commun Integr Biol*. 4:409–412.

Chen, C.Y., and F.M. Brodsky. 2005. Huntingtin-interacting protein 1 (Hip1) and Hip1-related protein (Hip1R) bind the conserved sequence of clathrin light chains and thereby influence clathrin assembly in vitro and actin distribution in vivo. *J. Biol. Chem.* 280:6109–6117. http://dx.doi.org/10.1074/jbc.M408454200

Damke, H., T. Baba, D.E. Warnock, and S.L. Schmid. 1994. Induction of mutant dynamin specifically blocks endocytic coated vesicle formation. *J. Cell Biol.* 127:915–934. http://dx.doi.org/10.1083/jcb.127.4.915

Deborde, S., E. Perret, D. Gravotta, A. Deora, S. Salvarezza, R. Schreiner, and E. Rodriguez-Boulan. 2008. Clathrin is a key regulator of basolateral polarity. *Nature*. 452:719–723. http://dx.doi.org/10.1038/nature06828

Dictenberg, J.B., W. Zimmerman, C.A. Sparks, A. Young, C. Vidair, Y. Zheng, W. Carrington, F.S. Fay, and S.J. Doxsey. 1998. Pericentrin and γ-tubulin form a protein complex and are organized into a novel lattice at the centrosome. *J. Cell Biol.* 141:163–174. http://dx.doi.org/10.1083/jcb.141.1.163

Doxsey, S.J., P. Stein, L. Evans, P.D. Calarco, and M. Kirschner. 1994. Pericentrin, a highly conserved centrosome protein involved in microtubule organization. *Cell*. 76:639–650. http://dx.doi.org/10.1016/0092-8674(94)90504-5

Esk, C., C.Y. Chen, L. Johannes, and F.M. Brodsky. 2010. The clathrin heavy chain isoform CHC22 functions in a novel endosomal sorting step. *J. Cell Biol.* 188:131–144. http://dx.doi.org/10.1083/jcb.200908057

Feng, B., H. Schwarz, and S. Jesuthasan. 2002. Furrow-specific endocytosis during cytokinesis of zebrafish blastomeres. *Exp. Cell Res.* 279:14–20. http://dx.doi.org/10.1006/excr.2002.5579

Fu, W., W. Tao, P. Zheng, J. Fu, M. Bian, Q. Jiang, P.R. Clarke, and C. Zhang. 2010. Clathrin recruits phosphorylated TACC3 to spindle poles for bipolar spindle assembly and chromosome alignment. *J. Cell Sci.* 123:3645–3651. http://dx.doi.org/10.1242/jcs.075911

Gautier, A., A. Juillerat, C. Heinis, I.R. Corrêa Jr., M. Kindermann, F. Beaufils, and K. Johnsson. 2008. An engineered protein tag for multiprotein labeling in living cells. *Chem. Biol*. 15:128–136. http://dx.doi.org/10.1016/j.chembiol.2008.01.007

Gerald, N.J., C.K. Damer, T.J. O'Halloran, and A. De Lozanne. 2001. Cytokinesis failure in clathrin-minus cells is caused by cleavage furrow instability. *Cell Motil. Cytoskeleton*. 48:213–223. http://dx.doi.org/10.1002/1097-0169(200103)48:3<213::AID-CM1010>3.0.CO;2-V

Gergely, F., C. Karlsson, I. Still, J. Cowell, J. Kilmartin, and J.W. Raff. 2000. The TACC domain identifies a family of centrosomal proteins that can interact with microtubules. *Proc. Natl. Acad. Sci. USA*. 97:14352–14357. http://dx.doi.org/10.1073/pnas.97.26.14352

Gergely, F., V.M. Draviam, and J.W. Raff. 2003. The ch-TOG/XMAP215 protein is essential for spindle pole organization in human somatic cells. *Genes Dev.* 17:336–341. http://dx.doi.org/10.1101/gad.245603

Hannak, E., M. Kirkham, A.A. Hyman, and K. Oegema. 2001. Aurora-A kinase is required for centrosome maturation in *Caenorhabditis elegans*. *J. Cell Biol.* 155:1109–1116. http://dx.doi.org/10.1083/jcb.200108051

Heerssen, H., R.D. Fetter, and G.W. Davis. 2008. Clathrin dependence of synaptic-vesicle formation at the *Drosophila* neuromuscular junction. *Curr. Biol.* 18:401–409. http://dx.doi.org/10.1016/j.cub.2008.02.055

Huang, F., A. Khvorova, W. Marshall, and A. Sorkin. 2004. Analysis of clathrin-mediated endocytosis of epidermal growth factor receptor by RNA interference. *J. Biol. Chem.* 279:16657–16661. http://dx.doi.org/10.1074/jbc.C400046200

Hubner, N.C., A.W. Bird, J. Cox, B. Splettstoesser, P. Bandilla, I. Poser, A. Hyman, and M. Mann. 2010. Quantitative proteomics combined with BAC TransgeneOmics reveals in vivo protein interactions. *J. Cell Biol.* 189:739–754. http://dx.doi.org/10.1083/jcb.200911091

Joshi, S., S. Perera, J. Gilbert, C.M. Smith, A. Mariana, C.P. Gordon, J.A. Sakoff, A. McCluskey, P.J. Robinson, A.W. Braithwaite, and M. Chircop. 2010. The dynamin inhibitors MiTMAB and OcTMAB induce cytokinesis failure and inhibit cell proliferation in human cancer cells. *Mol. Cancer Ther.* 9:1995–2006. http://dx.doi.org/10.1158/1535-7163.MCT-10-0161

Juillerat, A., T. Gronemeyer, A. Keppler, S. Gendreizig, H. Pick, H. Vogel, and K. Johnsson. 2003. Directed evolution of O6-alkylguanine-DNA alkyltransferase for efficient labeling of fusion proteins with small molecules in vivo. *Chem. Biol.* 10:313–317. http://dx.doi.org/10.1016/S1074-5521(03)00068-1

Kawamoto, K., F. Herz, R.C. Wolley, A. Hirano, H. Kajikawa, and L.G. Koss. 1979. Flow cytometric analysis of the DNA distribution in human brain tumors. *Acta Neuropathol.* 46:39–44. http://dx.doi.org/10.1007/BF00684802

Keppler, A., M. Kindermann, S. Gendreizig, H. Pick, H. Vogel, and K. Johnsson. 2004. Labeling of fusion proteins of O6-alkylguanine-DNA alkyltransferase with small molecules in vivo and in vitro. *Methods*. 32:437–444. http://dx.doi.org/10.1016/j.ymeth.2003.10.007

Kuriyama, R., and G.G. Borisy. 1981. Microtubule-nucleating activity of centrosomes in Chinese hamster ovary cells is independent of the centriole cycle but coupled to the mitotic cycle. *J. Cell Biol.* 91:822–826. http://dx.doi.org/10.1083/jcb.91.3.822

Lehtonen, S., M. Shah, R. Nielsen, N. Iino, J.J. Ryan, H. Zhou, and M.G. Farquhar. 2008. The endocytic adaptor protein ARH associates with motor and centrosomal proteins and is involved in centrosome assembly and cytokinesis. *Mol. Biol. Cell*. 19:2949–2961. http://dx.doi.org/10.1091/mbc.E07-05-0521

Lemercier, G., S. Gendreizig, M. Kindermann, and K. Johnsson. 2007. Inducing and sensing protein—protein interactions in living cells by selective cross-linking. *Angew. Chem. Int. Ed. Engl.* 46:4281–4284. http://dx.doi.org/10.1002/anie.200700408

Lin, C.H., C.K. Hu, and H.M. Shih. 2010. Clathrin heavy chain mediates TACC3 targeting to mitotic spindles to ensure spindle stability. *J. Cell Biol.* 189:1097–1105. http://dx.doi.org/10.1083/jcb.200911120

Lingle, W.L., and J.L. Salisbury. 1999. Altered centrosome structure is associated with abnormal mitoses in human breast tumors. *Am. J. Pathol.* 155:1941–1951. http://dx.doi.org/10.1016/S0002-9440(10)65513-7

Lingle, W.L., K. Lukasiewicz, and J.L. Salisbury. 2005. Deregulation of the centrosome cycle and the origin of chromosomal instability in cancer. *Adv. Exp. Med. Biol.* 570:393–421. http://dx.doi.org/10.1007/1-4020-3764-3_14

Liu, S.H., M.C. Towler, E. Chen, C.Y. Chen, W. Song, G. Apodaca, and F.M. Brodsky. 2001. A novel clathrin homolog that co-distributes with cytoskeletal components functions in the trans-Golgi network. *EMBO J.* 20:272–284. http://dx.doi.org/10.1093/emboj/20.1.272

Liu, Z., and Y. Zheng. 2009. A requirement for epsin in mitotic membrane and spindle organization. *J. Cell Biol.* 186:473–480. http://dx.doi.org/10.1083/jcb.200902071

Marumoto, T., S. Honda, T. Hara, M. Nitta, T. Hirota, E. Kohmura, and H. Saya. 2003. Aurora-A kinase maintains the fidelity of early and late mitotic events in HeLa cells. *J. Biol. Chem.* 278:51786–51795. http://dx.doi.org/10.1074/jbc.M306275200

Montagnac, G., A. Echard, and P. Chavrier. 2008. Endocytic traffic in animal cell cytokinesis. *Curr. Opin. Cell Biol.* 20:454–461. http://dx.doi.org/10.1016/j.ceb.2008.03.011

Mori, D., Y. Yano, K. Toyo-oka, N. Yoshida, M. Yamada, M. Muramatsu, D. Zhang, H. Saya, Y.Y. Toyoshima, K. Kinoshita, et al. 2007. NDEL1 phosphorylation by Aurora-A kinase is essential for centrosomal maturation, separation, and TACC3 recruitment. *Mol. Cell. Biol.* 27:352–367. http://dx.doi.org/10.1128/MCB.00878-06

Moskowitz, H.S., J. Heuser, T.E. McGraw, and T.A. Ryan. 2003. Targeted chemical disruption of clathrin function in living cells. *Mol. Biol. Cell*. 14:4437–4447. http://dx.doi.org/10.1091/mbc.E03-04-0230

Näthke, I.S., J. Heuser, A. Lupas, J. Stock, C.W. Turck, and F.M. Brodsky. 1992. Folding and trimerization of clathrin subunits at the triskelion hub. *Cell*. 68:899–910. http://dx.doi.org/10.1016/0092-8674(92)90033-9

Nigg, E.A., and J.W. Raff. 2009. Centrioles, centrosomes, and cilia in health and disease. *Cell*. 139:663–678. http://dx.doi.org/10.1016/j.cell.2009.10.036

Niswonger, M.L., and T.J. O'Halloran. 1997. A novel role for clathrin in cytokinesis. *Proc. Natl. Acad. Sci. USA*. 94:8575–8578. http://dx.doi.org/10.1073/pnas.94.16.8575

Okamoto, C.T., J. McKinney, and Y.Y. Jeng. 2000. Clathrin in mitotic spindles. *Am. J. Physiol. Cell Physiol.* 279:C369–C374.

Peset, I., and I. Vernos. 2008. The TACC proteins: TACC-ling microtubule dynamics and centrosome function. *Trends Cell Biol.* 18:379–388. http://dx.doi.org/10.1016/j.tcb.2008.06.005

Piehl, M., and L. Cassimeris. 2003. Organization and dynamics of growing microtubule plus ends during early mitosis. *Mol. Biol. Cell*. 14:916–925. http://dx.doi.org/10.1091/mbc.E02-09-0607

Pihan, G.A., A. Purohit, J. Wallace, R. Malhotra, L. Liotta, and S.J. Doxsey. 2001. Centrosome defects can account for cellular and genetic changes that characterize prostate cancer progression. *Cancer Res.* 61:2212–2219.

Prekeris, R., and G.W. Gould. 2008. Breaking up is hard to do - membrane traffic in cytokinesis. *J. Cell Sci.* 121:1569–1576. http://dx.doi.org/10.1242/jcs.018770

Radulescu, A.E., and D. Shields. 2012. Clathrin is required for postmitotic Golgi reassembly. *FASEB J.* 26:129–136. http://dx.doi.org/10.1096/fj.10-167684

Royle, S.J. 2012. The role of clathrin in mitotic spindle organisation. *J. Cell Sci.* 125:19–28. http://dx.doi.org/10.1242/jcs.094607

Royle, S.J., and L. Lagnado. 2006. Trimerisation is important for the function of clathrin at the mitotic spindle. *J. Cell Sci.* 119:4071–4078. http://dx.doi.org/10.1242/jcs.03192

Royle, S.J., N.A. Bright, and L. Lagnado. 2005. Clathrin is required for the function of the mitotic spindle. *Nature*. 434:1152–1157. http://dx.doi.org/10.1038/nature03502

Sager, P.R., P.A. Brown, and R.D. Berlin. 1984. Analysis of transferrin recycling in mitotic and interphase HeLa cells by quantitative fluorescence microscopy. *Cell*. 39:275–282. http://dx.doi.org/10.1016/0092-8674(84)90005-9

Salisbury, J.L., K.M. Suino, R. Busby, and M. Springett. 2002. Centrin-2 is required for centriole duplication in mammalian cells. *Curr. Biol.* 12:1287–1292. http://dx.doi.org/10.1016/S0960-9822(02)01019-9

Sardon, T., I. Peset, B. Petrova, and I. Vernos. 2008. Dissecting the role of Aurora A during spindle assembly. *EMBO J.* 27:2567–2579. http://dx.doi.org/10.1038/emboj.2008.173

Schweitzer, J.K., E.E. Burke, H.V. Goodson, and C. D'Souza-Schorey. 2005. Endocytosis resumes during late mitosis and is required for cytokinesis. *J. Biol. Chem.* 280:41628–41635. http://dx.doi.org/10.1074/jbc.M504497200

Shimizu, H., I. Nagamori, N. Yabuta, and H. Nojima. 2009. GAK, a regulator of clathrin-mediated membrane traffic, also controls centrosome integrity and chromosome congression. *J. Cell Sci.* 122:3145–3152. http://dx.doi.org/10.1242/jcs.052795

Sluder, G., and C.L. Rieder. 1985. Centriole number and the reproductive capacity of spindle poles. *J. Cell Biol.* 100:887–896. http://dx.doi.org/10.1083/jcb.100.3.887

Straight, A.F., C.M. Field, and T.J. Mitchison. 2005. Anillin binds nonmuscle myosin II and regulates the contractile ring. *Mol. Biol. Cell*. 16:193–201. http://dx.doi.org/10.1091/mbc.E04-08-0758

Telzer, B.R., and J.L. Rosenbaum. 1979. Cell cycle-dependent, in vitro assembly of microtubules onto pericentriolar material of HeLa cells. *J. Cell Biol.* 81:484–497. http://dx.doi.org/10.1083/jcb.81.3.484

Thompson, H.M., A.R. Skop, U. Euteneuer, B.J. Meyer, and M.A. McNiven. 2002. The large GTPase dynamin associates with the spindle midzone and is required for cytokinesis. *Curr. Biol.* 12:2111–2117. http://dx.doi.org/10.1016/S0960-9822(02)01390-8

Thompson, H.M., H. Cao, J. Chen, U. Euteneuer, and M.A. McNiven. 2004. Dynamin 2 binds gamma-tubulin and participates in centrosome cohesion. *Nat. Cell Biol.* 6:335–342. http://dx.doi.org/10.1038/ncb1112

Vassilopoulos, S., C. Esk, S. Hoshino, B.H. Funke, C.Y. Chen, A.M. Plocik, W.E. Wright, R. Kucherlapati, and F.M. Brodsky. 2009. A role for the CHC22 clathrin heavy-chain isoform in human glucose metabolism. *Science*. 324:1192–1196. http://dx.doi.org/10.1126/science.1171529

von Kleist, L., W. Stahlschmidt, H. Bulut, K. Gromova, D. Puchkov, M.J. Robertson, K.A. MacGregor, N. Tomilin, A. Pechstein, N. Chau, et al. 2011. Role of the clathrin terminal domain in regulating coated pit dynamics revealed by small molecule inhibition. *Cell*. 146:471–484. http://dx.doi.org/10.1016/j.cell.2011.06.025

Wakeham, D.E., L. Abi-Rached, M.C. Towler, J.D. Wilbur, P. Parham, and F.M. Brodsky. 2005. Clathrin heavy and light chain isoforms originated by independent mechanisms of gene duplication during chordate evolution. *Proc. Natl. Acad. Sci. USA*. 102:7209–7214. http://dx.doi.org/10.1073/pnas.0502058102

Warner, A.K., J.H. Keen, and Y.L. Wang. 2006. Dynamics of membrane clathrin-coated structures during cytokinesis. *Traffic*. 7:205–215. http://dx.doi.org/10.1111/j.1600-0854.2005.00377.x

Wilbur, J.D., C.Y. Chen, V. Manalo, P.K. Hwang, R.J. Fletterick, and F.M. Brodsky. 2008. Actin binding by Hip1 (huntingtin-interacting protein 1) and Hip1R (Hip1-related protein) is regulated by clathrin light chain. *J. Biol. Chem.* 283:32870–32879. http://dx.doi.org/10.1074/jbc.M802863200

Wilde, A., and F.M. Brodsky. 1996. In vivo phosphorylation of adaptors regulates their interaction with clathrin. *J. Cell Biol.* 135:635–645. http://dx.doi.org/10.1083/jcb.135.3.635

Ybe, J.A., S. Perez-Miller, Q. Niu, D.A. Coates, M.W. Drazer, and M.E. Clegg. 2007. Light chain C-terminal region reinforces the stability of clathrin heavy chain trimers. *Traffic*. 8:1101–1110. http://dx.doi.org/10.1111/j.1600-0854.2007.00597.x

Young, A., J.B. Dictenberg, A. Purohit, R. Tuft, and S.J. Doxsey. 2000. Cytoplasmic dynein-mediated assembly of pericentrin and gamma tubulin onto centrosomes. *Mol. Biol. Cell*. 11:2047–2056.